An Experimental Investigation of Fracture at an Interface between Two Epoxies

Thesis by

Satoshi Sugawara

In Partial Fulfillment of the Requirements

for the Degree of

Aeronautical Engineer

California Institute of Technology

Pasadena, California

1994

(submitted September 27, 1993)

Acknowledgments

This work was made possible through the support, guidance and encouragement of many people. Chief among these was my advisor, Professor Wolfgang G. Knauss, who provided scientific direction when needed, valuable suggestions when appropriate, and continuous support throughout my graduate studies.

I would like to acknowledge principal support from the Hitachi, Ltd. under the study-abroad program of 1993. The direct and indirect assistance provided by the organization are greatly appreciated.

I wish to acknowledge the significant contribution made towards this research effort by Mr. John M. Bowen. Both the specimen preparation technique and the experimental procedure outlined here are largely the outgrowth of Mr. Bowen's work with Solithane during his graduate studies from 1990-1992.

Special thanks are in order to Dr. Philippe Geubelle, who provided valuable insight and guidance to use the FEAP analysis code on many occasions. I also wish to acknowledge the assistance of Mr.Hongbin Lu and Mr.Weinong Chen, graduate students at GALCIT. Mr.Hongbin Lu provided helpful guidance to use and control the MTS testing machine and Mr.Weinong Chen provided assistance in using the strain gauges.

I would also like to acknowledge the skills and services of Mr. Joe Haggerty and Mr.Phil Wood of the Aeronautics Machine Shop, and Mr.Petros Arakelian of Solid Mechanics in Aeronautics. Their quick assistance in machining the specimens used in this study and the assembly of the testing apparatus for manufacturing the epoxy specimens were very helpful.

Abstract

The growth of a crack located at the interface between two linearly elastic solids is investigated experimentally. The requirements for the test pieces are strong bonding between the two materials, a well-defined, planar interface, and a pronounced difference in the stiffness between the two materials. To attain these requirements, castable liquid epoxy resins are used. It is demonstrated that the manufacturing process, which follows previously established procedures for the bi-material solid composed of Solithane, is also applicable for epoxy. To investigate the toughness of the interface crack, the measurement of crack speed and the estimation of stress intensity factors are carried out for several different temperatures. Master curves of crack speed for either of the two materials and for the bi-material are presented. The experimentally obtained fracture toughness data are compared with the expected values by Knauss's model (1971). By varying the mode mixity at the crack tip, it is found that the crack might advance by kinking into the soft material or by propagating along the interface itself, depending on the applied loading conditions. Although the number of data points is small, the fracture data gathered from tests performed at two different temperatures indicate that rate effects significantly influence the kinking behavior. Crack tip speeds after kinking are also recorded.

Table of Contents

Copyright ii

Acknowledgments iii

Abstract v

Table of Contents vi

List of Figures viii

List of Tables x

1. Introduction 1

2. Rate dependent fracture toughness 3

3. Linearly elastic interfacial fracture mechanics 8

4. Specimen manufacturing optimization 12

4.1 Selection of epoxy resin 12

4.2 Selection of curing agents 12

4.3 Sample preparation 13

4.3.1 Epoxy block form 14

4.3.2 Volume of each component 15

4.3.3 Manufacturing process 15

4.4 Tensile test specimen 17

4.5 Strip biaxial specimens 18

5. Experimental procedure 28

5.1 Uniaxial deformation properties 28

5.1.1 Stress and strain 28

5.1.2 Poisson's ratio 29

5.1.3 Stress relaxation 29

5.2 Fracture properties 30

5.2.1 Fracture specimen 30
5.2.2 The load frame assembly 31
5.2.3 Crack speed measurement 31
5.2.4 Measurement of the kinking direction 32
6. Numerical analysis 38
7. Results 42
7.1 Uniaxial deformation properties 42
7.1.1 Stress-strain relation 42
7.1.2 Poisson's ratio 45
7.1.3 Uniaxial tensile stress relaxation 46
7.2 Fracture properties 47
7.2.1 Crack speed measurements 47
7.2.1.1 Homogeneous material 47
7.2.1.2 Bi-material interface 48
7.2.1.3 Comparison with theoretical solution 49
7.2.2 Observation of crack propagation near the interface 50
7.3 Kinking behavior of the bi-material joint 51
7.3.1 Observations on the kink geometry 51
7.3.2 Observations on crack speed after kinking 52
8. Conclusions 73
References 75

List of Figures

Number		Page
3.1	Geometry of the bi-material problem	11
4.1	Apparatus for mixing epoxy	23
4.2	Exploded view of the two-piece mold	24
4.3	The configuration of tensile specimens	25
4.4	Geometry of the bi-material fracture specimen	26
4.5	Lower half of the mold with epoxy and Teflon tape, top view	27
5.1	Arrangement of the strain gauge on the specimen	33
5.2	Modelling of specimen subjected to constant applied displacements	34
5.3	Photograph of the load frame assembly with a mounted specimen	35
5.4	Determination of the loading angle θ	36
5.5	Measurement of experimentally observed kink angle	37
6.1	Details of the finite element discretization	41
7.1	Stress-strain relation (case8)	55
7.2	Stress-strain relation (case9)	55
7.3	Stress-strain relation (case1)	56
7.4	Stress-strain relation (case8)	56
7.5	Stress-strain relation (case10)	57
7.6	Poisson's ratio vs. axial strain obtained by strain gauge	58
7.7	Uniaxial tensile stress relaxation	59
7.8	Uniaxial tensile stress relaxation (with cracks)	59
7.9	Example of date analysis for determining crack speed	60
7.10	Crack velocity as a function of temperature reduced strain	61

7.11 Crack velocity as a function of stress intensity factors at several temperatures……62
7.12 Master curve of crack speed derived from figure 7.11…… 63
7.13 Crack velocity as a function of temperature reduced strain……64
7.14 Crack velocity as a function of stress intensity factors at several temperatures……64
7.15 Master curve of crack speed derived from figure 7.14…… 65
7.16 The material Ψ functions for the two solids……65
7.17 The Ψ function for bi-material interface fracture…… 66
7.18 Crack propagation speed as a function of the stress intensity factor……66
7.19 Geometry of the homogeneous fracture specimen manufactured through sandwiching process……67
7.20 Comparison between crcak speed and applied strain……68
7.21 Observed kinking behavior of the interface crack…… 69
7.22 Observed crack tip position and crcak tip velocity after kinking(25°C)……70
7.23 Observed crack tip position and crcak tip velocity after kinking(40°C)……71

List of Tables

Number Page

4.1 Typical physical properties 21

4.2 Manufacturing condition for epoxy blocks 22

6.1 Material properties 40

7.1 Summary of stiffness moduli 53

7.2 Dimension of specimen 53

7.3 Comparison of stiffness moduli 54

7.4 Comparison between loading angle and crcak speed 54

1. Introduction

There are many situations in the aerospace industry where parts are joined by mechanical fasteners or adhesive and are intended to act also as failure barriers. In solid rocket propellant rocket motors the line/insulation combination should be invulnerable to cracks that may start in the propellant. For, if such cracks penetrate the insulation or should separate the insulation from the motor case, burn-through of the motor case will result. These types of problems are not unique to the aerospace industry but occur in many branches of engineering. Geubelle (1993) pointed out that they occur in the epitaxial layers of semiconductors in the electronics industry. For these circumstances the failure prediction and prevention should be well established.

For metallic structures the associated design problems are dealt with effectively through fracture mechanics principles. For polymers joined adhesively the knowledge related to these kinds of problems is virtually non-existent. While we know that designs are fracture resistant if one employs "tough" materials, any uncertainty arises primarily from the complications associated with time dependent material behavior of the adherent materials. Practically speaking, according to reports by Knauss (1988), errors in the computed stresses of 5-10% may result in errors in estimated failure times on the order of factors of 10 or 100 (1-2 orders of magnitude) or more.

In (visco)elastic polymers, two uncertainties are significant for the behavior of a crack. First, it is the realistic definition of the stress and deformation state at the tip of the crack. Second, the effect of two (or more) material functions on the crack growth behavior introduces

uncertainty. Stated alternatively, the investigation of the second uncertainty might be a search for an understanding and prediction of the dependence on the material properties for crack growth between two polymer materials if the crack growth behavior in a monolithic polymer solid is understood.

In order to study the motion of cracks near interfaces it is necessary to understand their motion through a monolithic solid of either properties. For this purpose one needs to measure the rate of crack speed in (visco)elastic solids of either of the two materials. Moreover, to study crack growth near interfaces, it is necessary to produce specimens which allow for a planar interface so that standard analytical tools may be brought to bear on the data analysis.

To provide the background required for the rate dependent fracture toughness evaluation, the theory of viscoelastic bondline decohesion is described in Chapter 2. In Chapter 3, the primary concepts of linearly elastic fracture mechanics for the interfacial crack problem are briefly cited. It is imperative for this study to generate specimens with high interfacial fracture strength; the preparation of specimens is described in Chapter 4. This is followed by a description of the test fixture and test procedure described in Chapter 5. The analysis of the crack tip stresses is accomplished numerically through finite element analysis using the code FEAP. In this analysis, the crack tip stress intensity factors are determined according to a plane stress, linearly elastic formulation. Details of that analysis are not presented here, but the analysis model and conditions on analysis are presented in Chapter 6. The test results are presented and discussed in Chapter 7.

2. Rate dependent fracture toughness

The experimental program revealed that in some of the interfacial crack propagation experiments branching occured away from the interface. Knauss (1989) tentatively explained that the interface, though cast into the specimens in a "virgin state," may not represent the same molecular constitution across the interface as one would expect in a material all cast from one homogeneous piece. Another explanation by Knauss states that the interface strength in the bi-material solid is less than the intrinsic strength of either of the two solids.

In order to interpret the consequence of this lower interface strength on the crack propagation behavior, the growth of a crack at an interface is given by a rate dependent fracture toughness proposed by Knauss (1974). In this chapter this relation is cited and explained briefly.

In 1974, Knauss proposed a rate-dependent fracture toughness relation for homogeneous solid. For plane stress, by the relation for the stress intensity factor K and crack speed $\dot{a}$ through

$$2\,D^{\infty}\,\Theta\left(\frac{\alpha}{\dot{a}}\right)K^{2}=\Gamma \qquad (2.1)$$

$D^{\infty}=D(\infty)$: long-term equilibrium uniaxial creep compliance of the two adhering homogeneous solid.

Θ : viscoelasticity function defined below. [Eq.(2.4)]

α : a characteristic, microstructual parameter.

a : crack length.

$\dot{a}$: crack tip speed.

Γ : the intrinsic, constant surface energy required for unit crack extension into the material in the limit of zero crack speed.

Eq. (2.1) is valid for constant crack speed.

For instance, in a polyurethane, α was identified with the Dugdale / Barenblatt parameter such that,

$$\alpha \equiv \frac{\pi K^2}{8\sigma_0^2} \tag{2.2}$$

in which σ_0 denotes the ultimate cohesive stress of the solid.

Eq. (2.1) strictly applies only in the case of constant crack speed. However, this equation gives a good approximation for variable crack speeds $\dot{a}(t)$

$$\frac{1}{K}\frac{\partial K}{\partial t} << \frac{\dot{a}(t)}{2\alpha(t)}. \tag{2.3}$$

In this equation, K=K(t) is the time-varying stress intensity factor [Knauss and Dietmann (1970), Knauss (1976)]. The viscoelasticity function Θ is defined by

$$\Theta(s) = E^{\infty}\int_0^1 \left\{ D_0 F(\rho) - \int_s^1 \Delta D\left[s\cdot(r-\rho)\frac{dF(r)}{dr}dr \right] \right\} d\rho \tag{2.4}$$

where $E^{\infty} = \frac{1}{D^{\infty}}$ is the long-term or equilibrium uniaxial modulus of elasticity, F(r) is a non-dimensional function related to the crack tip stress field and deformation.

An approximation [Knauss, 1974] of the above equation is given by,

$$\Theta(s) \equiv \frac{1}{2} E^{\infty} D(s) \tag{2.5}$$

Accordingly, Eq.(2.1) is rewritten (approximately) as

$$D\left(\frac{\alpha}{\dot{a}}\right) K^2 = \Gamma . \tag{2.6}$$

For the purpose of an approximation, it is convenient to introduce here the function $\varphi\left(\frac{\alpha}{\dot{a}}\right)$, defined by

$$\varphi\left(\frac{\alpha}{\dot{a}}\right) \equiv \frac{1}{2\,\Theta\left(\frac{\alpha}{\dot{a}}\right)} \tag{2.7}$$

so that Eq. (2.1) can now be rewritten as

$$D^{\infty} K^2 = \frac{K^2}{E^{\infty}} = \Gamma\ \varphi\left(\frac{\alpha}{\dot{a}}\right). \tag{2.8}$$

For the case of two nearly incompressible viscoelastic solids joined together, according to the definition shown by Knauss (1971), the rate of unbonding along the interface is (approximately) governed by,

$$\left[D_1^{\infty}\Theta_1\left(\frac{\alpha}{\dot{a}}\right) + D_2^{\infty}\Theta_2\left(\frac{\alpha}{\dot{a}}\right)\right]K^2 = \Gamma_i \qquad (2.9)$$

where D_1^{∞} *and* D_2^{∞} : the long term creep compliances of the two jointed solids. The subscript denotes the two different materials.

$\Theta_1(s)$ *and* $\Theta_2(s)$: the appropriate viscoelastic functions of Eq. (2.4).

K : stress intensity factor such as $K = \sqrt{K_I^2 + K_{II}^2}$.

K_I and K_{II} :Mode I and Mode II stress intensity factor respectively.

Γ_i : the intrinsic strength of the interface (intrinsic fracture energy).

Since it is not clear as to how the length scale (α) is related to those associated with the two homogeneous materials by themselves, it is assumed that the size scales for the two solids considered here are sufficiently close so as not to pose a problem of first order. In effect, it is assumed that the interface failure is governed approximately by the same size parameter as for the two materials separately. This is based on the fact that the molecular structures of each material are not very different. It would be appropriate to examine the validity of this relation with a relatively more different set of materials than the materials used by Bowen (1992).

By analogy of Eq. (2.8), the rate dependent function appropriate to the interface itself, which is denoted by φ_i, is given by [Bowen &Knauss, 1992],

$$\varphi_i\left(\frac{\alpha}{\dot{a}}\right)=\frac{D_1^{\infty}+D_2^{\infty}}{2D_1^{\infty}\Theta_1\left(\frac{\alpha}{\dot{a}}\right)+2D_2^{\infty}\Theta_2\left(\frac{\alpha}{\dot{a}}\right)}=\frac{D_1^{\infty}+D_2^{\infty}}{\left(\frac{D_1^{\infty}}{\varphi_1(s)}\right)+\left(\frac{D_2^{\infty}}{\varphi_2(s)}\right)}. \tag{2.10}$$

Hence, Eq. (2.9) becomes

$$\frac{1}{2}\left(D_1^{\infty}+D_2^{\infty}\right)K^2=\Gamma_i\,\varphi_i\left(\frac{\alpha}{\dot{a}}\right). \tag{2.11}$$

It is postulated that (2.11) describes fracture along the interface between two viscoelastic solids where the rate-dependent function φ_i embodies the material rate effects of the interface separation.

3. Linearly elastic interfacial fracture mechanics

In this experimental study, the objective is to shed light on the broadly posed question regarding the extent to which linear analysis is able to represent physical reality. In this chapter, the stress intensity factor for the bi-material case is briefly explained under the two assumptions that (i) the loading angle parameters are maintained constant, (ii) a quasi-static crack growth conditions prevail.

Hutchinson, Mear and Rice (1987) and Rice (1988) proposed that the local crack tip stress field for the semi-infinite interface crack can be written in the form,

$$\sigma_{\alpha\beta} = \Re e\left[K(2\pi r)^{-\frac{1}{2}}\left(\frac{r}{\ell}\right)^{i\varepsilon} \tilde{\sigma}_{\alpha\beta}(\theta)\right] \tag{3.1}$$

where r and θ are planar-polar coordinates centered at the tip of the crack as illustrated in Fig. 3.1, $i = \sqrt{-1}$ *and* $K = K_I + i\, K_{II}$ is the complex interface stress intensity factor. The "oscillation index" is defined by

$$\varepsilon = \frac{1}{2\pi}\ln\left(\frac{1-\beta}{1+\beta}\right) \tag{3.2}$$

which expresses the degree of dissimilarity exhibited by a particular material combination.

Following established notation, we use Dundur's mismatch parameters

$$\alpha = \frac{\mu_1(\kappa_2+1)-\mu_2(\kappa_1+1)}{\mu_1(\kappa_2+1)+\mu_2(\kappa_1+1)} = \frac{E_1^{'}-E_2^{'}}{E_1^{'}+E_2^{'}} \tag{3.3a}$$

$$\beta = \frac{\mu_1(\kappa_2-1)-\mu_2(\kappa_1-1)}{\mu_1(\kappa_2+1)+\mu_2(\kappa_1+1)} \tag{3.3b}$$

where subscripts 1 and 2 refer to the materials above and below the interface respectively (see Fig. 5.2), μ_ρ is the shear modulus, ν_ρ is the Poisson's ratio, . E_ρ is Young's modulus of material ρ respectively, $E^{'} = E$ in plane stress and $E/(1-\nu^2)$ in plane strain., $\kappa=(3-\nu)/(1+\nu)$ for plain stress and $3-4\nu$ for plain strain. Note that α and β vanish when the dissimilarity between the elastic properties of the two materials vanishes and that these parameters change sign when materials 1 and 2 are interchanged.

The full field expansion of the stresses at the tip of the interface crack yields, ahead of the crack tip (along the interface) [Sun and Jih, 1987]

$$\sigma_{22} + i\,\sigma_{12}\big|_{\theta=0} = \frac{1}{\sqrt{2\pi r}}(K_1 + iK_2)\left(\frac{r}{\ell}\right)^{i\varepsilon} \tag{3.4}$$

where K_α are the stress intensity factors of Eq. (3.1), ℓ is a characteristic length of the problem taken here to be the unit dimension (e.g., 1 cm).

In an homogeneous body, Eq. (3.4) becomes

$$\sigma_{22} + i\,\sigma_{12} = \frac{1}{\sqrt{2\pi r}}(K_I + iK_{II}). \tag{3.5}$$

It is important to note that the interfacial stress intensity factors, K_1 and K_2 are defined such that $K_1 \to K_I$ *and* $K_2 \to K_{II}$ when the dissimilarity

between the two materials vanishes ($\varepsilon = 0$). The ratio K_2/K_1 indicates the "mode mixity" at the crack tip ; this parameter is typically quantified through the "phase angle" $\gamma = \tan^{-1}\left(K_2/K_1\right)$.

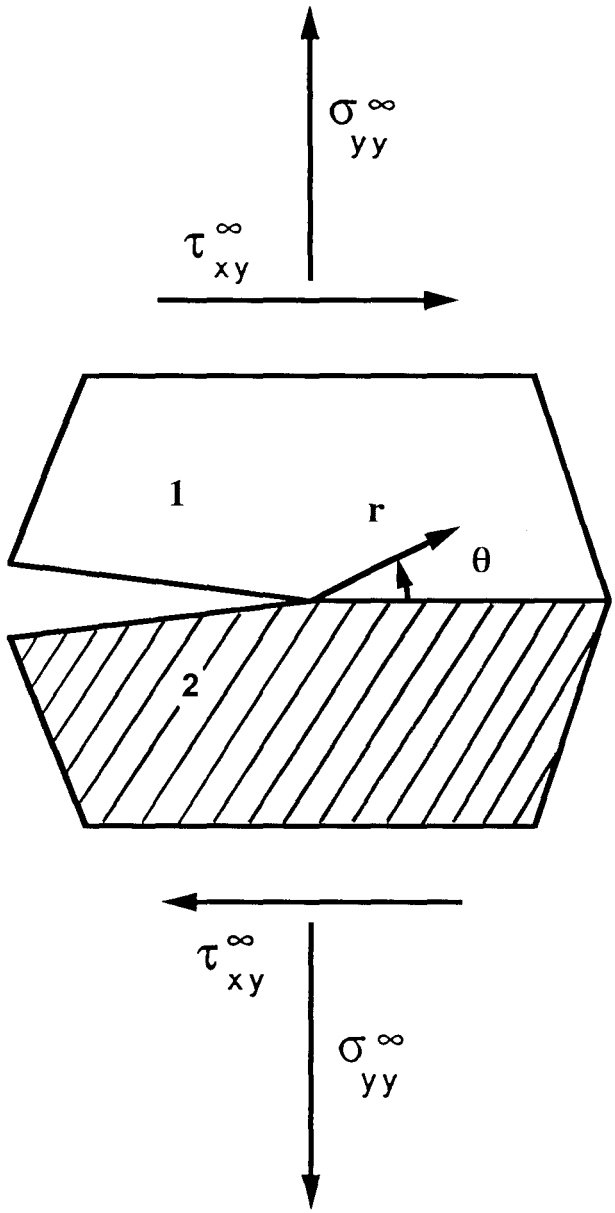

Figure 3.1 Geometry of the bi-material problem.

4. Specimen manufacturing optimization

In order to perform the experimental investigation, appropriate bi-material specimens are necessary. The requirements for the test pieces are that strong bonding exists between the two materials and that a well-defined, planar interface exist. Furthermore, the difference in the moduli (stiffness) of the materials should be as large as possible. In order to achieve different values for the moduli, liquid epoxy resin was used.

4.1 Selection of epoxy resin

The selection of the epoxy resins was based on the "Young's modulus" as achieved through epoxy formulation. The physical properties of some flexible epoxy resins stated in a catalog determined the kind of epoxy resins. The physical properties are summarized in Table 4.1. To satisfy the requirements described above, liquid epoxy resins such as D.E.R. 331[1] and D.E.R. 732[1] (shown in column A & B in Table 4.1) were tried. Since D.E.R. 732 modified the high viscosity of D.E.R. 331 without affecting color of the cured compositions, these two epoxy resins were selected. By using these resins, the two different epoxies could be manufactured by adjusting the volume of resin and curing agent.

4.2 Selection of curing agents

Epoxy resins may be polymerized with a variety of curing agents. Selecting the proper curing agent is conditioned by the application, pot life required, cure conditions, condition of handling, and physical properties

---

[1] Trade marks for epoxy from the Dow Chemical Company.

desired. Once a curing agent is selected , one determines the relative weight percentage per active H stoichiometry (or phr) in accordance with the recommended value from the supplier (Dow Chemical Company).

In order to determine the curing agent with ease of handling in mind, small samples were made, with dimensions of 56 x 18 mm, containing curing agents as shown in Table 4.1. Thus, D.E.H. 20 was chosen as the curing agent because it offered a large difference of the stiffness for the two materials, low viscosity (like water) and fast curing times at room temperature (gel formation at room temperature, (RT), plus 1 to 2 hours at 100 °C). D.E.H. 20 belongs to the family of the Aliphatic Polyamines and its chemical name is diethylene triamine (DETA). Preliminary manufacturing of samples with D.E.H.20, showed that bubbles which developed during the reaction process had sufficient time to reach the surface resulting in specimens with no porosity.

4.3 Sample preparation

In order to optimize the interfacial strength of the bi-material specimens, one needs to investigate the gel time and thus, what will be related to as the "*time interval* ." The optimal conditions to design and manufacture satisfactory bi-material specimens, is given by varying the *time interval.* Two types of epoxy resins such as the 70/30 combination and 50/50 combinations were used. The former combination signifies 70 weight percentages (wt.%) of D.E.R.331 and 30 wt.% of D.E.R. 732combination while the latter refers to 50 wt.% of D.E.R. 331 and 50 wt.% of D.E.R. 732 combination.

We use the two "hard" and "soft" materials depending on the relative stiffness of the materials. The 70/30 composition represents "hard" material and the 50/50 composition is "soft" material.

To bond the two materials, they were cured together. This was achieved by setting the optimal "*time interval* " before pouring the second material on the first material. If this "*time interval* " is too short, a non-planar interface will be formed because the first cast material is too soft to resist deformations when the second material is poured on it. Although a hard interfacial surface is obtained from a well cured solid, the bonding condition of the two materials is unknown. Therefore, finding the optimal time interval is necessary to make the proper specimens for fracture testing.

To find the optimal "*time interval,* " the tensile properties were studied as a function of the "*time interval.*" This range was varied from 0 to 25 hours. A well cured solid was obtained for a time interval of 25 hours. The features of total 13 cases in the range are shown in Table 4.2. From the results of the tensile property tests, the optimal "*time interval* " was selected.

4.3.1 Epoxy block form

Since this epoxy is cast as a liquid, surface tension prevents the possibility of directly casting a bi-material specimen with a planar interface in sheet form in a two-step procedure. Hence a bi-material specimen is cast in block form in order to minimize the severity of surface tension effects over the area of the interface. The fully cured bi-material block can then be cut or otherwise machined into the desired fracture specimen geometry.

4.3.2 Volume of each component

The weight of the epoxy resins, curing agents, and dyes are determined in accordance with stoichiometric ratios. First, one calculates the amine hydrogen equivalent weight (AHEW) of the curing agent. In this case that was 20.6. Second, one calculates the epoxide equivalent weight (EEW) of the two components. These were 187 for D.E.H. 331 and 320 for D.E.H. 732 respectively. Finally, one calculates the weight percentages of the composition that are summarized as follows :

Hard material (70/30 composition)		Soft Material (50/50 composition)	
D.E.R. 331	63.8 wt.%	D.E.R. 331	46.0 wt.%
D.E.R. 732	27.3 wt.%	D.E.R. 732	46.0 wt.%
D.E.H. 20	8.8 wt.%	D.E.H. 20	8.0 wt.%
Dye*	0.1 wt.%		
Total	100 wt. %	Total	100 wt.%

* Dye[2] was added to the hard material to facilitate identifying the interface between the hard and the soft materials because the original materials were slightly amber, but otherwise.

4.3.3 Manufacturing process

J.M.Bowen (1992) described the manufacturing process for Solithane 113. Here we follow the same procedure except for the temperature range and time period of each manufacturing step: The bi-material specimen was prepared in two steps. The hard material was prepared first. The weights

---

[2] Commassie Brilliant Blue R-250, Gibco BRL, Life Technologies, Inc.

of hard material reported in 4.3.2 were added in a 500 ml Erlenmeyer flask. The weight percentage of 0.1 dye was added to the epoxy mixture to provide a satisfactory color tone.

The flask was maintained at 37 ±1 °C through a water bath, and the contents was mixed in a vacuum for 8 minutes. Throughout the mixing process, the vacuum was relaxed periodically and nitrogen gas was introduced briefly in order to release the bubbles that developed inside the epoxy during the reaction (Fig. 4.1).

After completion of the mixing phase, the epoxy was transferred into the lower half of a two-piece mold. This mold had been treated with a fluorocarbon release agent[3] in order to facilitate the eventual removal of the cured sample. The fully assembled molds were an aluminum parallelepiped with the internal dimensions of 75 mm x 75 mm x 120 mm, the last dimension denoting the overall height respectively (Fig. 4.2).

The mold and its batch of the hard material were then maintained at room temperature for the optimal "*time interval* ." The soft material was prepared according to a procedure analogous to that used for the hard material, except for the use of the dye. The natural clear color of this layer was preserved in order to differentiate between the two compositions in the final specimen.

After the soft material had completed its mixing cycle (10 minutes at 38°C), it was poured into the mold on top of the partially cured hard material. The two compositions were then allowed to fully cure together in the mold, according to the following heat cycle : 12 hours at RT, followed by 60 minutes at 100 °C. After the completion of the curing cycle, the oven was shut off and the sample was allowed to cool inside the closed oven

---

[3] Miller-Stephenson Chemical Company, Inc., TFE Release Agent/Dry Lubricant.

overnight. The cure time was determined by trial and error. The criterion to judge whether the curing cycle is achieved or not is the size and the distribution of bubbles. After the full curing of the epoxy, there were quite a few small bubbles, their diameters are (about) less than 0.5 mm, in the peripheral area. However it was hard to eliminate the bubbles generated in the center area of the block due to the unbalanced heat distribution through the curing period. This portion of the block was discarded later. The color of the interior of the block will change to reddish brown because of auto catalytic heatup when the temperature is high and the cure time is long. If the temperature is low and the time is short, bubbles will remain inside the epoxy.

Once the mold has cooled to room temperature, it is dismantled and the epoxy removed. The dimensions of the dual-epoxy block were 75 mm x 75 mm x 62 mm, the last dimension denoting the overall height.

4.4 Tensile test specimen

In order to obtain the uniaxial deformation properties, the constant deformation rate of the hard, soft, and bi-material were measured. For this purpose, thirteen blocks were manufactured under different conditions, which are shown in Table 4.2. From each block, five different specimens were cut. The configuration of the specimens are shown in Fig. 4.3. In the wider flat area (9 mm) of specimen type "C," a strain gauge was attached to measure Poisson's ratio. The flat length (30 mm) was intended for attaching the extensometer.

The thin slices or sheets (3 mm) were cut from the blocks with a milling machine. The slices were cut perpendicular to the interface. Both end sheets bordering on opposite walls of the mold were discarded because

of the surface tension-induced curvature of the interface. To make specimens with flat interfaces (type B in Fig. 4.3), we selected that region in which the interface of the two materials was flat even if the whole interface of the block was not totally planar. Next, the test piece was maintained at 115 ° C for 3 hours after machining in order to release any possible residual stress, which might have arisen in the machining process.

4.5 Strip biaxial specimens

Mazor and Bowen (1989) first studied suitable bi-material test geometries by using Solithane 113.[4] They tested several geometries, discussed several manufacturing techniques, and recommended a thick sheet specimen for the bi-material fracture study. This type of specimen, illustrated in Fig. 4.4, has dimensions that have been designed to provide a practical approximation to the semi-infinite strip, for which the stress intensity factor is independent of the crack length.

In order to make a crack at the interface of both materials, a thin sheet of Teflon is employed. The procedure to form the crack is as follows: Since the Teflon strip will define gross location of the interfacial crack, its planarity and placement are critical. To ensure planarity of the Teflon and to retard the natural tendency of the thin sheet to curl, the Teflon was passively "ironed" for several hours prior to the following procedure: it was cut to size and then maintained 3 hours at 210°C in between two smooth steel plates at a high load (24.5 kN).

Next, after casting the hard material into the lower half of a two-piece mold, the Teflon strip was placed on the hard material in the position shown in Fig. 4.5. After the Teflon had been put in place with tweezers, it

[4] Solithane 113 is the trade name for a polyurethane elastomer manufactured by Morton Thiokol, Inc.

was carefully "brushed" with the tips of the tweezers in order to free air bubbles that might be trapped between the lower surface of the Teflon and the hard material. Then, the upper half of the mold was securely fastened to the lower half using the bolts

Next, following passage of the proper "*time interval,*" the soft material was poured into the fully assembled mold on top of the partially cured hard material and the Teflon sheet. The Teflon prevented the two compositions from coming into contact and hence provided an area where no bonding across the interface occurs. This region defined a coarse "crack" in the final specimens. To obtain the desired edge crack with a requisite sharp crack front, the 5 mm ligament of material behind the Teflon in the fully cured, cut sheets would be mechanically cut prior to the fracture tests.

When the test piece had been cooled, thin aluminum loading grips were bonded with an RTV silicone rubber adhesive[5] to the specimen. On each face of the specimen, these grips were made parallel to be and symmetrical about the interface such that the test specimen had a "height" of 4.0 cm
(c.f. Fig. 4.4). Next, the holes required for pins used to load the specimen during testing were drilled through the grips and the underlying epoxy.

Before testing, the 5.0 mm ligament of epoxy behind the crack, which was defined by the Teflon stripe as shown in Fig. 4.5, was cut with a razor blade. Finally, using the load frame described in the next chapter, the crack was forced to propagate along the interface for 2-3 mm so that a natural crack tip, located exactly at the interface[6] was obtained. This

---

[5] General Electric Company, Silicone Products Division, RTV108.
[6] To locate the crack tip on the interface, the pre-crack of the bimaterial were formed with loading angle of $\theta = 65.16^{\circ}$.

procedure eliminated the influence of the Teflon sheet near the crack tip. At this point, the bi-material specimen preparation was complete. The sheet -type homogeneous test pieces were composed of either hard or soft material, and which were used in the crack speed measurement, and were prepared in the same procedure described above.

Table 4.1 Typical physical properties.[1]

Resin Blend[4]	A	B	C	D	E	F	G	H	I	J	K
	70-331 30-732	50-331 50-732	30-331 70-732	100-331	70-331 30-732	100-331	70-331 30-732	100-331	70-331 30-732	100-331	100-438
Curing Agent	DEH20	DEH20	MDA[2]	MDA[2]	NMA[2]	NMA[2]	BF_3 MEA	BF_3 MEA	Polyamide	Polyamide	BF_3 MEA
phr[3]	9.5	8.4	23	26	87.5	87.5	3	3	43	43	3
Tensile Strength (MPa)	42.75	9.65	61.70	70.32	73.36	58.43	44.30	28.78	33.30	54.47	25.51
Tensile Modulus (GPa)	1.72	0.138	2.70	2.48	3.08	2.96	2.44	2.77	1.67	2.59	3.59

[1] Dow Chemical Company, Improved Elongation, Flexibility, and Impact in Cured Resins.
[2] MDA : Methylene Dianiline, NMA: Nadic Methyl Anhydride.
[3] Parts per hundred parts (resin).
[4] 30-732 stands for 30 wt% of D.E.R. 732, 70-331 stands for 70 wt% of D.E.R.331 and 100-438 stands for 100 wt% of D.E.N 438.

Table 4.2 Manufacturing condition for epoxy blocks.

Case Number	Resin Temp (°C)[1]	Time Interval (min. or hr)[2]
1	38	0-5 min.(N.F.I.)[3]
2	38	15 min.(N.F.I.).
3	38	30 min.(N.F.I.).
4	40	30 min.(N.F.I.)
5	38	45 min.(N.F.I.).
6	38	60 min.(N.F.I.).
7	38	60 min.(F.I.)[3]
8	38	70 min.(N.F.I.)
9	38	75 min.(F.I.)
10	38	25 hr (F.I.)
11	44	30 min.(N.F.I.)
12	32	40 min.(N.F.I.)
13	32	60 min.(N.F.I.)

1Temperature of resins just before pouring into mold.

2Time interval between pouring 70/30 resin and 50/50 resin into mold.

3 N.F.I. : not overall planar surface; F.I. : overall planar interface surface.

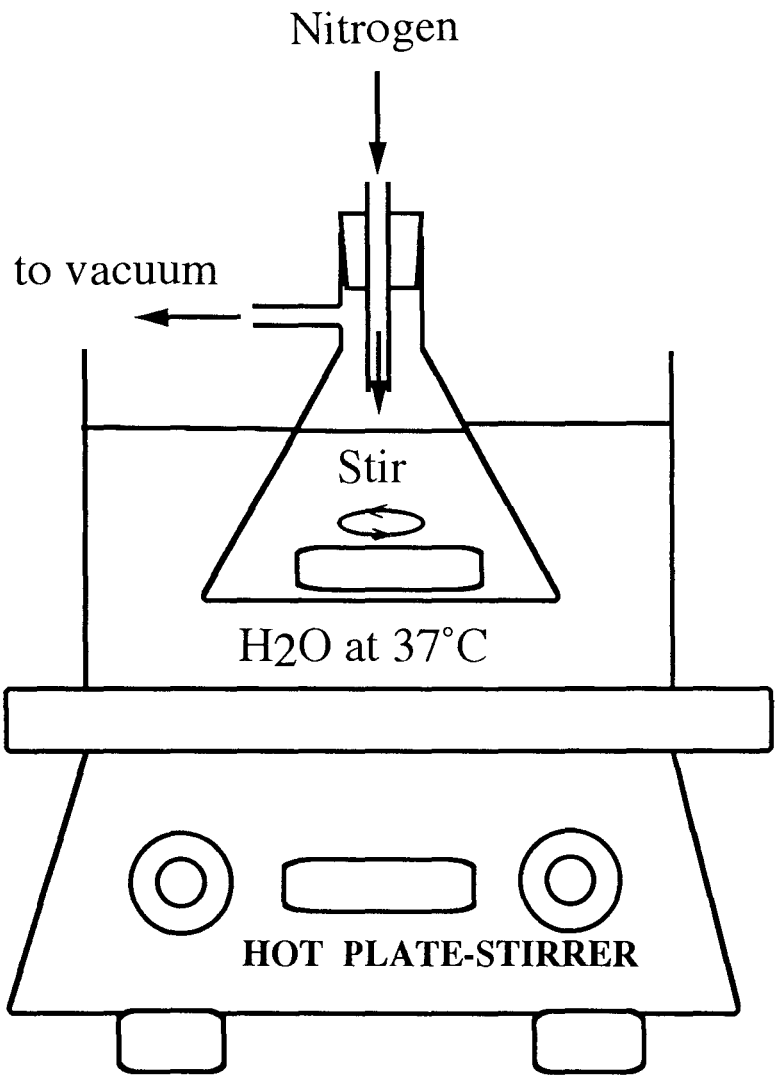

Figure 4.1 Apparatus for mixing epoxy.

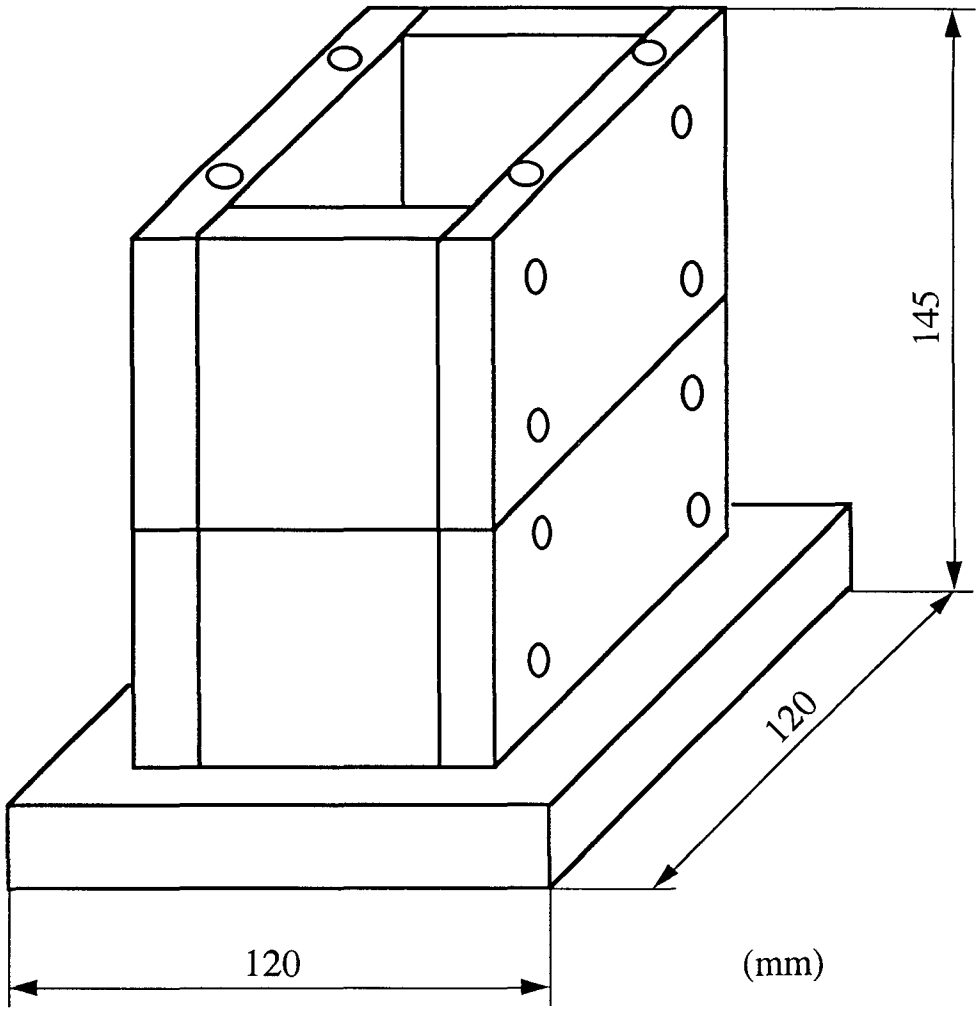

Figure 4.2 Exploded view of the two-piece mold.

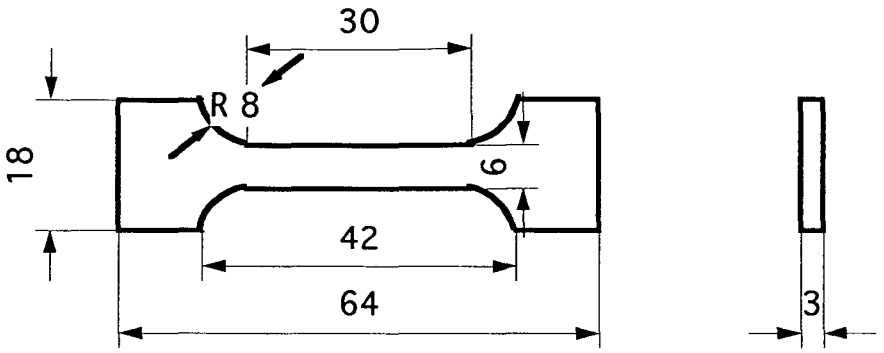

TYPE A-1 : Hard material (composed of 70/30 combination).
TYPE A-2 : Soft material (composed of 50/50 combination).
(a) For stress-strain relation measurement.

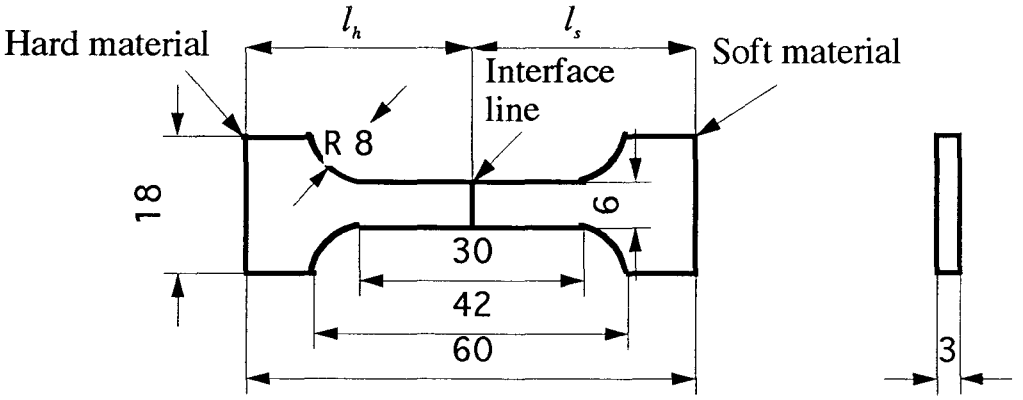

(b) For stress-strain relation measurement. (TYPE B)

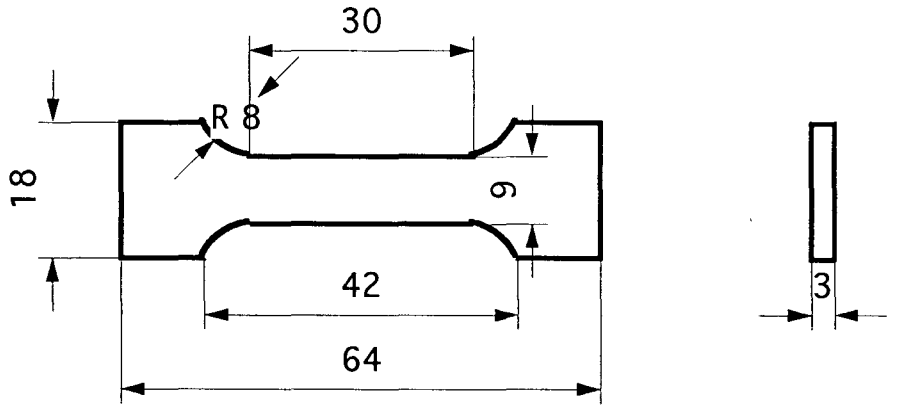

TYPE C-1 : Hard material (composed of 70/30 combination).
TYPE C-2 : Soft material (composed of 50/50 combination).
(c) For the stiffness modulus and Poisson's ratio measurement.

All dimensions in mm.

Figure 4.3 The configuration of tensile specimens.

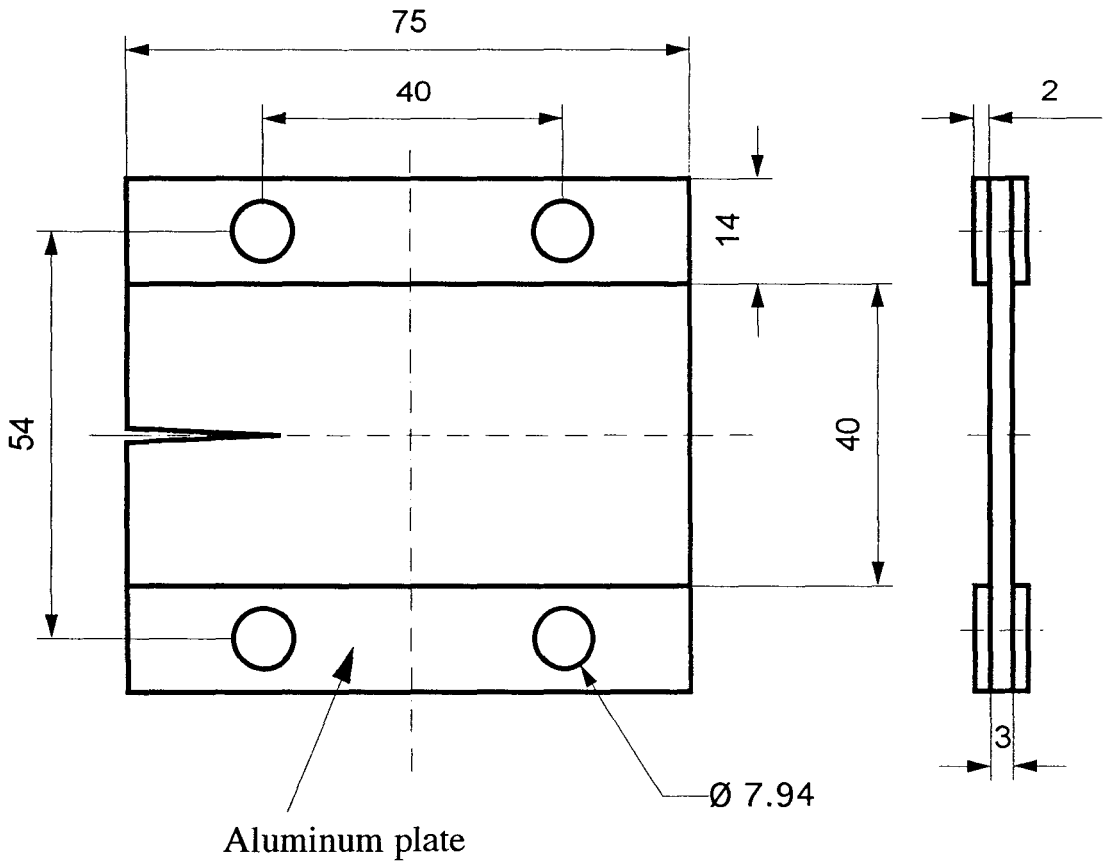

All dimensions in mm.

Figure 4.4 Geometry of the bi-material fracture specimen.

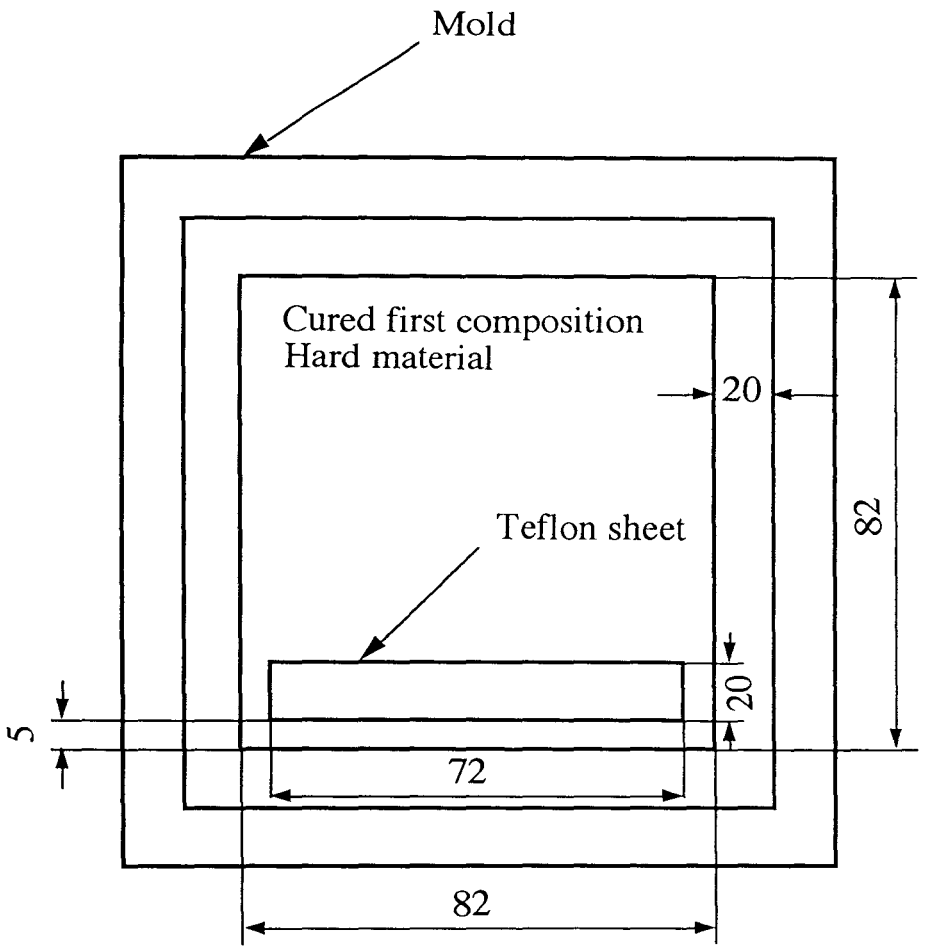

All dimensions in mm.

Figure 4.5 Lower half of the mold with epoxy and Teflon tape, top view.

5. Experimental procedure

It is convenient to separate the experimental procedure into two sections. The first, Chapter 5.1, is concerned with the uniaxial deformation properties. In that section, the procedure to obtain the constant deformation rate and Poisson's ratio with the tensile test specimen are explained. In the second part of this chapter, Chapter 5.2, the procedure to obtain the fracture properties with the strip biaxial specimens are described. The second part of the procedure is the same as the procedure used in an earlier study using Solithane 113[1] by Bowen (1989-1992).

5.1 Uniaxial deformation properties

The measurements of uniaxial deformation properties are necessary in order to determine separately for reference purposes the behavior of the two materials involved. In this section, first, the experimental procedures for getting the stress and strain relation and the constant deformation rate of the specimens are explained. Then, the procedures for obtaining the Poisson's ratio and stress relaxation behavior of the specimens are reported.

5.1.1 Stress and strain

The stress and strain values of each specimen were measured with a MTS testing machine[2] to calculate the constant deformation rate of the specimens.

---

[1] Solithane is the trade name for a polyurethane elastomer manufactured by Morton Thiokol, Inc.

[2] The axial-torsional load unit model number used in this experiment was 358.10. The actuator model number and transducer model number was 358.xx and 11019 respectively with the following load limits, axial : 3300 lb, torsional : 1500 in-lb.

The applied load was controlled in accordance with the output of the strain value. The strain was monitored by the output from the extensometer attached in the specimens. The strain ranges used in this experiment were 0 to 1.2 % for the hard and soft materials and 0 to 1.06 % for the bi-material. These values were set by trial and error to avoid breaking the test piece. The strain rate applied to the specimen was 1.77×10^{-2} % / sec. at room temperature. During the application of the load, the displacement, strain, and load values (which are converted to the stress values afterward) were measured in 1 second intervals. These data were then stored in the computer, which was connected to the MTS testing machine.
The "MASS COMP" computer uses the UNIX based digital data acquisition system. For the conversion of stress, the cross-section area of each specimen was measured in advance using calipers that had ±0.0254 mm (1 mil) accuracy.

5.1.2 Poisson's ratio

To determine Poisson's ratio of each material, the relation between the vertical and horizontal strain values was measured simultaneously. The geometry of the specimens composed of hard or soft material is shown in Fig. 4.3 (Type C-1 and Type C-2). The Strain gauges[3] were mounted on the surface of each specimen at 90° relative to each direction as shown in Fig. 5.1.

5.1.3 Stress relaxation

In order to assess the time dependent behavior of the two materials, their stress relaxation was measured. The load level was controlled by the

---

[3] Micro Measurement Co., Type EA-XX-062TT-350.

output of the strain value that was monitored by the extensometer attached on the specimen. The 1.0 % strain load of the material, which was measured in advance, was applied in 2 seconds and held constant for 30 minutes. During this period, the load values were measured and were stored in the computer in 1 second intervals.

5.2 Fracture properties

In order to study the motion of cracks near interfaces, it is necessary to understand their motion through a homogeneous solid on either side. For this purpose, one needs to measure the rate of crack speed not only in the bi-material but also in either of the two materials.

There are several issues connected with the topic of crack kinking from the interface. As pointed out by Knauss (1988) these were namely, the condition that determined whether a crack would kink away, the angle at which the kinked crack would propagate from the interface and the time required for the kinking to be completed. To investigate the conditions that result in kinking, the kinking angle as well as crack speed after kinking are observed and measured.

5.2.1 Fracture specimen

Fig. 5.2 illustrates the bi-material sheet type specimen. Fig. 5.2 (a) shows the physical test piece, subjected to an applied displacements U. The simplified bi-material specimen can be modeled as shown in Fig. 5.2 (b), in which the displacements are applied uniformly along the lengthwise boundaries of the specimen. Straining resulted from displacing the two long rails apart in a parallel manner so that in the central portion of the strip a homogeneous stress field resulted in which the crack propagate at a

constant rate because the crack tip conditions remained constant. In the experiment of crack speed measurement, the homogeneous sheet type specimens whose shape were similar to Fig. 5.2 (a) were used.

5.2.2 Load frame assembly

Fig. 5.3 shows the load frame assembly which is connected to the MTS testing machine. The crack tip loading is varied by changing the orientation of the specimen relative to the tension axis.

Bowen (1992) described the operation as follows: the orientation of the grips and the specimen is controlled by adjusting the vertical and horizontal positions of the eyes of the swing bolts. The swing bolts which have a pitch of 24 threads per inch can adjust precisely the vertical displacements and the angular rotation θ. The load frame shown in Fig. 5.3 provides the loading angle ; $-71.8^\circ \leq \theta \leq +71.8^\circ$.

5.2.3 Crack speed measurement.

The crack speed was obtained from the periodic measurement of the crack tip location. To find the load level for crack initiation, the load level was gradually increased till the breaking of specimens. Next, the load value was set at 70 % (for the soft material) and 97 % (for the hard material) of the breaking points. The position of the advancing crack tip was recorded with the aid of calipers and magnifying lens. The crack propagation speed was then obtained from these plots by taking the slope of the crack tip position-time trace.

To increase the opportunity of measurements, the specimens were renewed after each measurement. To eliminate the residual stresses

generated during the test, the used specimens were maintained at 80 °C (the soft material) and 105 °C (hard material) for one hour before reuse.

5.2.4 Measurement of the kinking direction

After the specimen was mounted onto the load frame, the loading angle θ was prescribed on the lower half of the load frame by suitably adjusting the two swing bolts (Fig. 5.4). The difference in height of the two corners of the lower lengthwise edge of the channel grip satisfies the following condition (Fig. 5.4).

$$\theta = \arcsin\left(\frac{h_2 - h_1}{10}\right) \quad \cdots\cdots (5.2.4.1)$$

where h_1 (cm) and h_2 (cm) as defined in Fig. 5.4.

To ensure that no significant restraining occurred as a result of mounting the specimen to the load frame, and to verify proper specimen alignment, the output of the load cell was monitored. Refinements in specimen alignment were performed until neither of the pins registered an applied load in excess of 1 N.

For each fracture test, the kink angle was measured by using an optical comparator. This device permitted the origin of the kink to be observed under sufficiently large magnification (≈20x). The kink angle ω is defined by the tangent to the crack extension at the point of deviation from the interface (Fig. 5.5); ω is then the angle between this ray and the plane of the interface. As shown in Fig. 5.5, this ω was measured positive counter-clockwise from the interface.

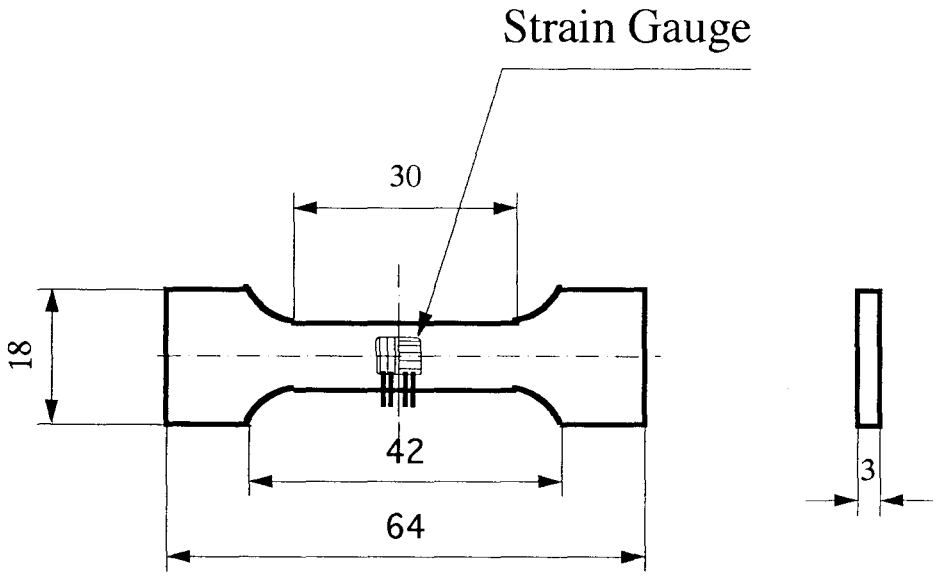

All dimensions in mm.

Figure 5.1 Arrangement of the strain gauge on the specimen.

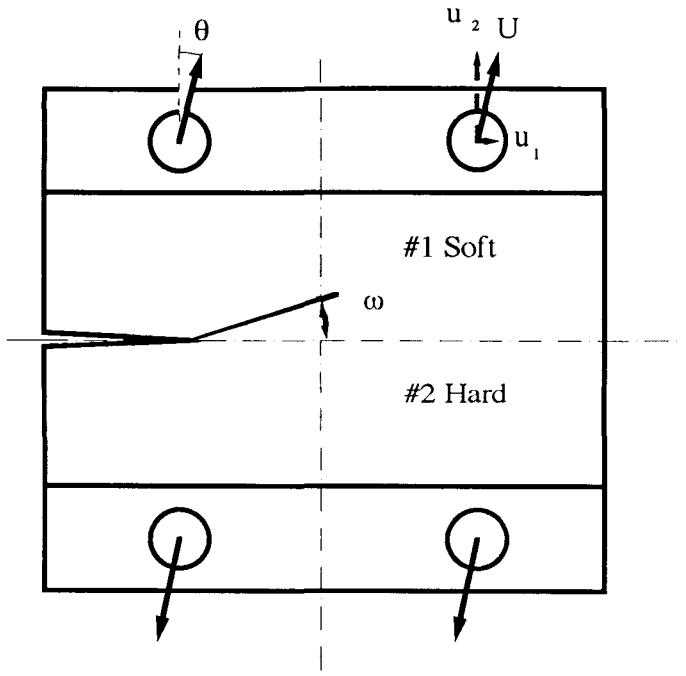

(a) Physical test piece.

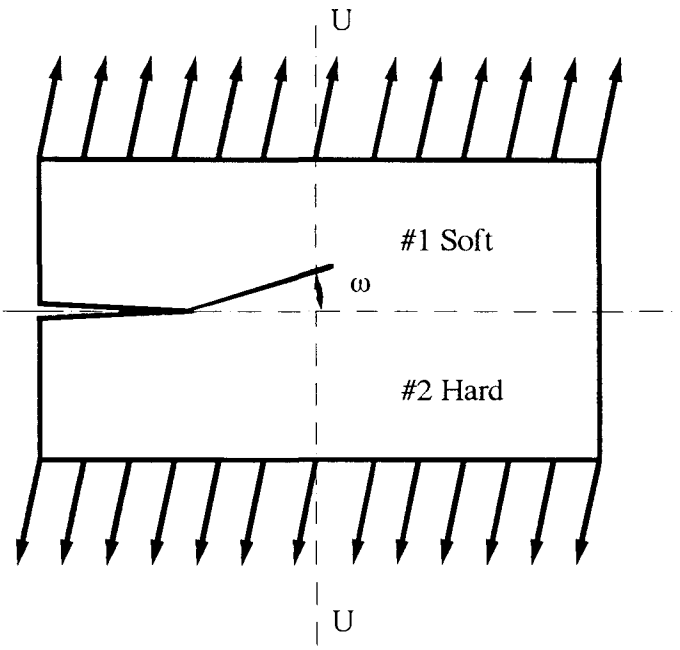

(b) Experimental and analytical model.

Figure 5.2 Modeling of a specimen subjected to constant applied displacements.

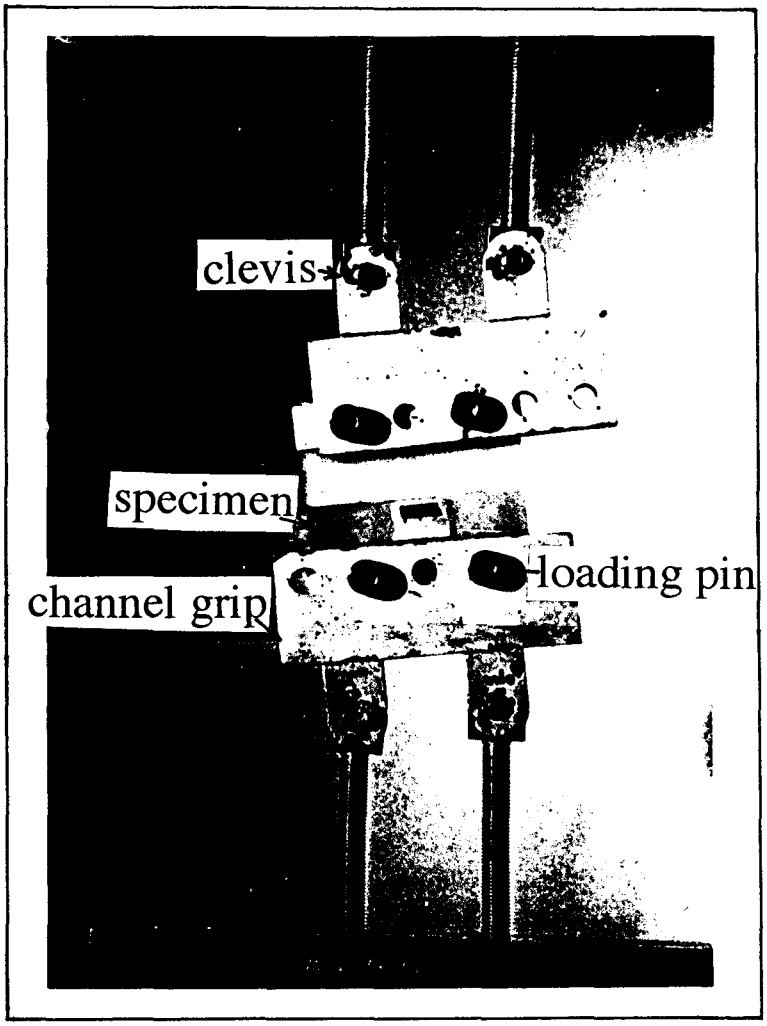

Figure 5.3 Photograph of the load frame assembly with a mounted specimen.

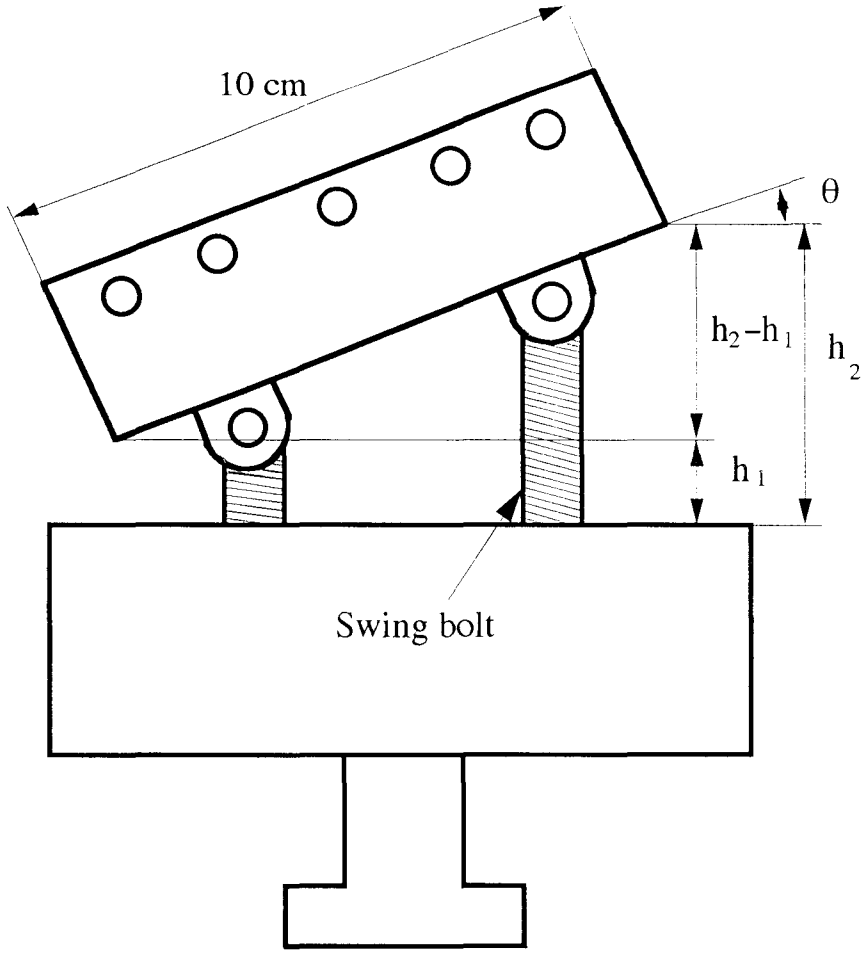

Figure 5.4 Determination of the loading angle θ.

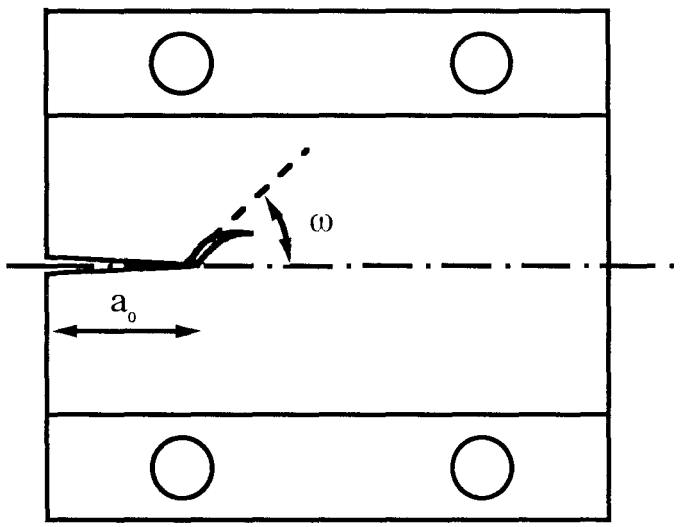

Figure 5.5 Measurement of experimentally observed kink angle.

6. Numerical analysis

In order to evaluate the experimental results one needs the crack tip stress field characterization in terms of the stress intensity. The Finite Element Method (FEM) is used to compute the near tip stress fields using the assumption of linear elasticity and plane stress conditions.

The program code for the Finite Element Method, "FEAP," employs the semi-energetic numerical scheme proposed by Matos (1989). This technique combines the nodal crack tip opening displacements with the values of the J-integral to determine the two stress intensity factors K_1 and K_2. For the homogeneous and the bi-material stress intensity factor calculation, the scheme proposed by Geubelle (1991) was used.

Analysis procedure : The applied boundary displacements U, which is provided by the MTS testing machine, may be decomposed into components u_1 and u_2, representing displacements parallel and perpendicular to the plane of the interface, which are used in this analysis and are defined as

$$u_1 = U \sin\theta$$
$$u_2 = U \cos\theta. \qquad (6.1)$$

These values are prescribed along the entire length of the specimen edges in the numerical code. Hence, an arbitrary combination of far-field tension and shear loading can be prescribed by suitable adjustment of the loading angle θ in the experiment.

The finite element mesh consists of 3286 four-node elements concentrically focused at the crack tip as shown, for example, in Fig. 6.1. The material properties of the components are summarized in Table 6.1.

In the case of bi-materials, the Dundurs's mismatch parameters defined in Eq. (3.3) was used.

Table 6.1 Material properties[1].

Composition	hard material	soft material
Modulus (GPa)	2.38	0.198
Poisson's ratio	0.32	0.20

[1] The method of measurement is reported in Chapter 7, Section 7.1.2.

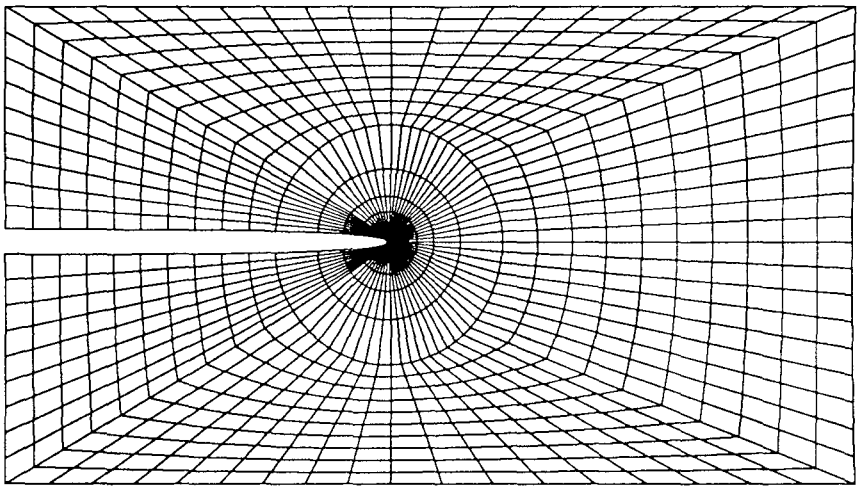

(a) Global view.

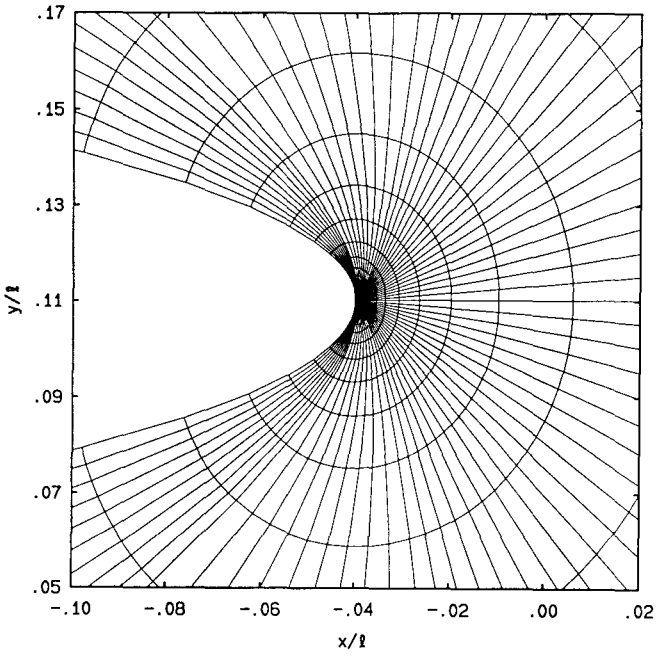

(b) Local view.

Figure 6.1 Details of the finite element discretization.

7. Results

The results are divided into two parts. The first part, delineated in Section 7.1, is concerned with the uniaxial deformation properties of the epoxy specimens. In the second part of this Chapter, Section 7.2, the fracture properties of the two homogeneous adherends and the bi-material interface are reported. In that section, the theory described in Chapter 2 is applied to bi-material and homogeneous specimens. In addition, the kinking behavior of the bi-material joint is presented and discussed. In that presentation, the influence of the shear/tension interaction on the direction of crack propagation relative to the interface is presented.

7.1 Uniaxial deformation properties

In this section, uniaxial deformation properties are examined with the tensile specimens illustrated in Fig. 4.3 to examine the physical properties of the epoxies. This study seemed necessary to determine separately for reference purposes the behavior of the two materials involved.

7.1.1 Stress-strain relation

The stress -strain relationship of all test pieces, which are summarized in Table 4.2, are reported. Some of the test results are shown in Figures 7.1 to 7.5. Throughout these figures, the ordinate denotes stress and the abscissa denotes strain.

Repeatability and breaking point : In Fig. 7.1, the hard material 1 denotes the test results of the hard material with residual stresses induced during the machining process. The existence of residual stress

could be confirmed by circularly polarized light. In order to relieve these stresses, the test piece was maintained at 115 °C for 3 hours after machining. The test results obtained after this treatment are shown for the hard material 2 in Fig. 7.1.

Constant deformation rate : From the experimental results, we can calculate a "stiffness parameter" (E^*) similar to the Young's modulus of each material. To calculate the stiffness parameter, all data of stress and strain at 0 to 0.6 %[1] strain were fitted by the root mean square method. The results are summarized in Table 7.1. In order to check the validity of the stiffness measurement for the bi-material conditions, define the effective bi-material stiffness strength

$$E_{effect} = \frac{\ell_h + \ell_s}{\frac{\ell_h}{E_h} + \frac{\ell_s}{E_s}} \quad \cdots\cdots (7.1.1.1)$$

where l_h is the length of hard material, l_s is the length of soft material as shown in Fig. 4.3, E_h is the stiffness modulus of hard material, and E_s is the stiffness modulus of the soft material. The coefficients of Eq. (7.1.1.1) are listed in Table 7.2 and calculated results are reported in Table 7.3.

Since E^* and E_{effect} are close to each other in Cases 8, 9 and 10[2], one can say that the bi-material specimens manufactured with this procedure have the sufficient characteristics desired for this research. From the above results, the stiffness moduli are 2.38 GPa for the hard material, 0.441 GPa for the bi-material and 0.198 GPa for the soft material respectively. The modulus of the hard material is 12 times higher and "effective" modulus of bi-material is 2.26 times higher than that of the soft material.

---

[1] This was because the linear relation between the stress and strain were observed in this region.

[2] Case numbers are defined in Table 4.2.

Fracture specimens with cure intervals of 0 to 5 minutes : Fig. 7.3 shows the results when the cure time interval is 0 and 5 minutes. This time interval was too short to form and bond a flat interface. Because of the mixing of both materials, no interface was formed and as a result, at 1.0 % strain the stress value of the bi-material is 2.23 times higher than that of the soft material and that of the hard material is only 45% of that of the fully cured one. (cf. Fig. 7.2)

Interface optimizations with a cure interval of 70 minutes: Fig. 7.4 shows the results when the cure time interval was 70 minutes. The time interval was still too short to get a flat interface, and the central portion of the hard material was swelled into the upper (soft) material after pouring the soft material on the hard one.

Interface optimizations with a cure interval of 75 minutes: Fig. 7.2 shows the results when the cure time interval was 75 minutes. From these results, one observes that the repeatability of the responses at 1.0% strain are 6% for the hard material and 8% for the soft one. Since the variation among these values were not significant, this heat treatment procedure was used to obtain the same effect on the stress-strain relationship for all tensile test specimens. As a reference, the strain levels for breaking the tensile test pieces were 1.2 % to 1.3% for the hard material, and 8.0 % to 8.2 % for the soft material. In this curing time interval, an entirely flat interface between the hard and the soft materials could be accomplished. It is of note that this time period is the most critical to form the flat interface in the entire curing process although the curing time difference from the above case is only 5 minutes.

Interface optimizations with a cure interval of 25 hours : Fig. 7.5 shows the results for the time interval of 25 hours. The reason for selecting the time interval of 25 hours was that it allowed full cure of the first (hard) material. The comparison of Fig. 7.2 and Fig. 7.5 shows that the stress-strain relationships are almost identical within the accuracy of this experiment. This means that even if the second (soft) material is cast on the fully cured first (hard) material, almost the same response is obtained as for the materials when the cure time interval was 75 minutes.

We conclude that the cure time interval should be equal to or longer than 75 minutes to get the desired difference of the stiffness moduli and planar interface for the fracture testing in the next part of the investigation.

7.1.2 Poisson's ratio

Fig. 7.6 (a) shows the results of Poisson's ratio vs. axial strain of the hard material. In this figure, the Poisson's ratio was calculated from the strain gauges aligned with both the tension and the transverse axes of the specimen. Since the usage of the grip holding the specimen is not appropriate for the polymer, the repeatability in the data is about 15-20 % at 0.6 % axial strain. From these results, considering the experimental accuracy, one can say that the Poisson's ratio of the hard material is 0.32. (This value was obtained by the least square fitting of the data over the 0.5 to 1.0% strain ranges, which were close to the strain level at crack initiation for the hard material.)

Fig. 7.6 (b) shows the results of Poisson's ratio vs. axial strain of the soft material. In the soft material, although we obtained the strain values from the gauges, we did not know how to interpret these values because it

depended on the axial strain. In the following investigation, we assume Poisson's ratio as 0.2[3].

7.1.3 Uniaxial tensile stress relaxation

In order to determine some estimate for the time dependence of the hard and soft material, the stress relaxation in both materials was measured. The extension imposed by the test machine was controlled by the output of the strain value which was monitored through an extensometer attached to the specimen. The load for 1.0 % strain was applied in 2 seconds and was measured for 30 minutes. During this period, the load values were stored in the computer in 1.0 second intervals. In the test result shown in Fig. 7.7, the upper line group stands for the hard material and the lower one for the soft material. Since the data below 10 seconds contains loading transients, they are not shown in this figure. The relaxation rates α[4] is 2.98 x10^{-3} (s^{-1}) for the hard material, 8.18 x10^{-3} (s^{-1}) for the soft material at 25°C. In order to examine the effect of crack on the relaxation of both materials, the similar measurements with the strip specimens were made. The results are shown in Fig. 7.8. The relaxation rate (α) is 3.07 x10^{-3} (s^{-1}) for the hard material, 6.41 x10^{-3} (s^{-1}) for the soft material at 30°C. At 20 seconds, the stiffness modulus ratio of the hard to soft materials is 8.0[5] without a crack and 7.7 at 30°C, 9.0 at 35°C and 10 at 40°C with the crack. Note that the stiffness modulus ratio of the hard to soft materials with the crack are less than that without the crack and the latter values show a dependence of temperature.

---

[3] The alternative way for this measurement should be considered the next time.

[4] The relaxation rates, α is defined by $\sigma = k_0 + k_1 \exp(-\alpha t)$ where σ is an applied stress, k_0 and k_1 are constants.

[5] Average values of both data at 25°C.

7.2 Fracture properties

In this section, fracture properties were recorded with the strip biaxial specimens illustrated in Fig. 4.4. Crack propagation speeds are a very sensitive function of stress intensity factors; the stress intensity factors are calculated with the FEAP code.

7.2.1 Crack speed measurements

7.2.1.1 Homogeneous material

Before determining the fracture speeds along or away from the interface, crack speed measurements on the individual components were made. For each given strain typically five (or six) measurements of the crack tip position and the corresponding times were made. These data were then computer-reduced by fitting a "least squares straight line" to them. A typical example of such a data reduction plot for each velocity is shown in Fig. 7.9. These types of measurements were repeated at four temperatures from 25 to 40 °C for the soft and the bi-materials, and at 35 to 50 °C for the hard materials.

Around 160 measurements were made of which about one third were found to lead to inconsistent results. The reason, most likely, was that the zero strain was not established correctly. In order to determine the strain accurately it was necessary to set the displacement precisely. In the beginning stages of the experiment, the center position of both holes in the aluminum plates shown in Fig. 4.4 was not correct. After making a special jig to locate the holes more precisely, this problem was alleviated.

Fig. 7.10 shows plots of crack propagation speeds at several temperatures as a function of the temperature reduced strain (which is

proportional to the stress intensity factor) for the soft materials and for the hard materials. Fig. 7.11 shows crack propagation speed as a function of stress intensity factors at several temperatures for the soft (a) and for the hard (b) materials. For this estimation, the applied loads were recorded with the corresponding times and used in the calculation of stress intensity factors[6].

The stiffness modulus (E^*) is proportional to the absolute temperature; we apply that temperature reduction to the strain for the purpose of constructing the crack propagation master curve. This data appears reasonably shiftable according to the normal time-temperature superposition principle and the resulting "master curves" are shown in Fig. 7.12 (a) and (b). Details in this estimation are reported by Knauss (1988).

7.2.1.2 Bi-material interface

For each given strain typically five measurements of the crack tip position and the corresponding times were made. The procedure to estimate the crack tip velocity is the same as for the homogeneous case. These measurements were repeated at four temperatures from 25 to 40 °C.

Around 60 measurements were made of which about one fourth were found to lead to inconsistent results. The reason, most likely, was that the same as in homogeneous cases. Fig. 7.13 shows a plot of the crack propagation speed as a function of the temperature reduced strain at several temperatures. Fig. 7.14 shows a plot of the crack propagation speed as a function of the stress intensity factors at several temperatures. In this

---

[6] In the FEAP code, the stiffness moduli were used. To include the stress relaxation effect (cf. Fig. 7.8) on the stress intensity factors from the FEAP code, the stress intensity factor from the FEAP code were converted by the assumption such that the stiffness modulus is proportional to the applied load.

measurement, the loading angle was set for θ =65.16 °[7] to propagate the crack just along the interface. The "master curve" shifted with the normal time-temperature superposition principle is shown in Fig. 7.15.

7.2.1.3 Comparison with theoretical solution

In this section, the master curve for homogeneous and bi-material obtained from the experiments are compared with the results derived from the rate dependent fracture toughness as explained in Chapter 2.

For the two homogeneous materials, the calculated value of the functions Ψ_1 and Ψ_2 by Eq. (2.8) are shown in Fig. 7.16. The combined values Ψ_i by Eq. (2.10) are shown in Fig. 7.17. In this calculation, the asymptotic stress intensity factor for the hard material, $K_{initial,hard} = 0.15\ MPa\sqrt{m}$; for the soft material, $K_{initial,soft} = 0.032\ MPa\sqrt{m}$; for the interface, $K_{initial,bi-material} = 0.032\ MPa\sqrt{m}$ were assumed. From Fig. 7.17, the intrinsic interface strength, explained in Chapter 2, is intermediate to those of the two homogeneous solids. The resulting rate dependent fracture toughness curve for the interface obtained by Eq. (2.10) is compared with the experimental data, "master curve" as shown in Fig. 7.18. In this figure, the solid line denotes the calculated results. Agreement between experimental data and analytical results indicates that this model is reasonably applicable to this problem.

---

[7] To set this angle, the loading angle of θ =71.8 ° (this is the maximum angle of this test fixture) was first tried. From this preliminary test, there was no kinking out of the crack from the interface line. To keep the consistent condition throughout the experiment, the loading angle of θ =65.16 ° was used. The effects of loading angle are explained in section 7.3.2.

7.2.2 Observation of crack propagation near the interface

The initial crack is formed initially by a Teflon strip sandwiched between the two homogeneous materials; it is, therefore, difficult to generate a true "virgin state" under this manufacturing process. Especially in the hard homogeneous solid, the residual stress distribution generated by the sandwiching process could not be eliminated in the peripheral interfacial area of the strip specimen [8] . Strictly speaking, this state is not "virgin state" of homogeneous materials. The effect of the above mentioned residual stress for the direction of moving crack should be investigated [9] .

Such a study seemed necessary in order to determine the effect of the sandwiching process on the crack for reference purposes. Fig. 7.19 shows the specimen geometry used in this study. The tests were carried out by the procedure used in the crack speed measurement until the size of propagation reached 4.93 mm for hard material and 9.27 mm for the soft material. The results show that the crack propagated parallel to the interfacial line and no crack kinking was observed in the two homogeneous materials. Fig. 7.20 shows comparison between crack speed and applied strain. In this figure, "crack along interface" denotes the results with the homogeneous fracture specimen as shown in Fig. 4.4 and "crack not along interface," denotes the results with the specimen manufactured through the sandwiching process as shown in Fig. 7.19. For the hard material (Fig. 7.19 (a)), one can say that a speed of crack along the interface tends to increase with the increase of applied strain but it keeps constant in the case of crack not along the interface. For the soft material (Fig. 7.19 (b)),

---

[8] To eliminate these stresses, the baking time and period were changed systematically. In the end, they were not eliminated until the heat distortion (at 160°C, 1 hours) in the hard material. On the other hand, it was easily eliminated in the soft material at 80 °C for 1 hours.

[9] The effect of geometry is not investigated in this study.

this tendency in the hard material is also observed. The reason of this observation is that the speed of crack located in the interface tends to accelerate with the increase of load level because of separation of the interface. For the same strain level the hard material, say 3.5% strain (this is a predicted value because that was not measured in Fig. 7.19 (a)), the speed of crack located in the interface might be bigger than that of the other case. In the soft material, the average value of speed is close to each other.

7.3 Kinking behavior of the bi-material joint

In this section experiments related to kinking of a crack away from the interface are documented.

7.3.1 Observations on the kink geometry

The kinking behavior of the bi-material joint was investigated at 25°C and, to a limited extent, at 40°C. Since an elevated temperature provides material rate effects that are higher than those at room temperature, it is expected that a comparison of the fracture behavior observed at these two temperatures will provide insight into the potential influence of rate effects on the kinking behavior of interface cracks. For consistency, the magnitude of the applied strain was maintained constant [10] and only the loading angle θ was permitted to vary from test to test.

The fracture behavior of the bi-material joint at 25°C and 40°C is presented in Fig. 7.21. Because of the difference of temperature, the material rate conditions are significantly different between the two datasets.

---

[10] Applied strain 5.0% at 25°C and 4.5% at 40°C.

Therefore, one concludes that rate effects can significantly affect the direction of crack propagation within the small strain range studied here.

7.3.2 Observations on crack speed after kinking

Although only a limited number of runs were carried out, these observations of crack speed after kinking are reported. First, under the relatively small loading angle, a crack initially propagates along the interface and then kinking occurred as shown in Figures 7.22 (a) and (b). This is because kinking is apparently a phenomenon that requires a certain time to be accomplished. In passing from an interface crack to the fully developed and kinked crack established at some distance away from the interface requires time under the relatively small loading angle.

A second important observation is that crack speeds tend to decrease after kinking at 25°C (Figures 7.22 (a)&(b)).This is because the magnitude of the gross "opening mode" stresses is less for large kink angles than for small ones, and the tendency for crack propagation is consequently diminished. However the above mentioned tendency can not be observed in the fracture data at elevated temperatures.

From these results one concludes that rate effects can significantly affect the crack speed after kinking behavior within the small strain range studied here.

Table 7.1 Summary of stiffness moduli.

Case number	hard material E_h (GPa)	soft material E_s (GPa)	bi-material E* (GPa)
Case1 (0-5 min.)	1.111	0.200	0.760
Case8 (70 min.)	2.380	0.120	0.206
Case9 (75 min.)	2.380	0.198	0.441
Case10 (25 hrs)	2.380	0.198	0.441

Table 7.2 Dimension of specimen.

Case number	length of hard material l_h (mm)	length of soft material l_s (mm)
Case1 (0-5 min.)	(31.85)[1)]	(31.85)[1)]
Case8 (70 min.)	27.99	31.94
Case9 (75 min.)	28.44	29.85
Case10 (25 hrs)	29.97	29.58

1) averaged value is adopted because there was no interface.

Table 7.3 Comparison of stiffness moduli.

Case number	experiment E* (GPa)	effective E_{effect} (GPa)	$\frac{E^*}{E_{effect}}$ (GPa)
Case1 (0-5 min.)	0.760	0.339	2.240
Case8 (70 min.)	0.206	0.216	0.954
Case9 (75 min.)	0.441	0.358	1.232
Case10 (25 hrs)	0.441	0.368	1.198

Table 7.4 Comparison between loading angle and crack speed[1].

Case number	θ (deg.)	(cm/min.)
Case1	13.50	0.031139
Case2	27.47	0.035804
Case3	65.16	0.081855

[1] Test conditions are as follows; temperature, 40°C; loading condition, 5.0% strain in 3sec.; specimen type, bi-material; kink angle, 0°.

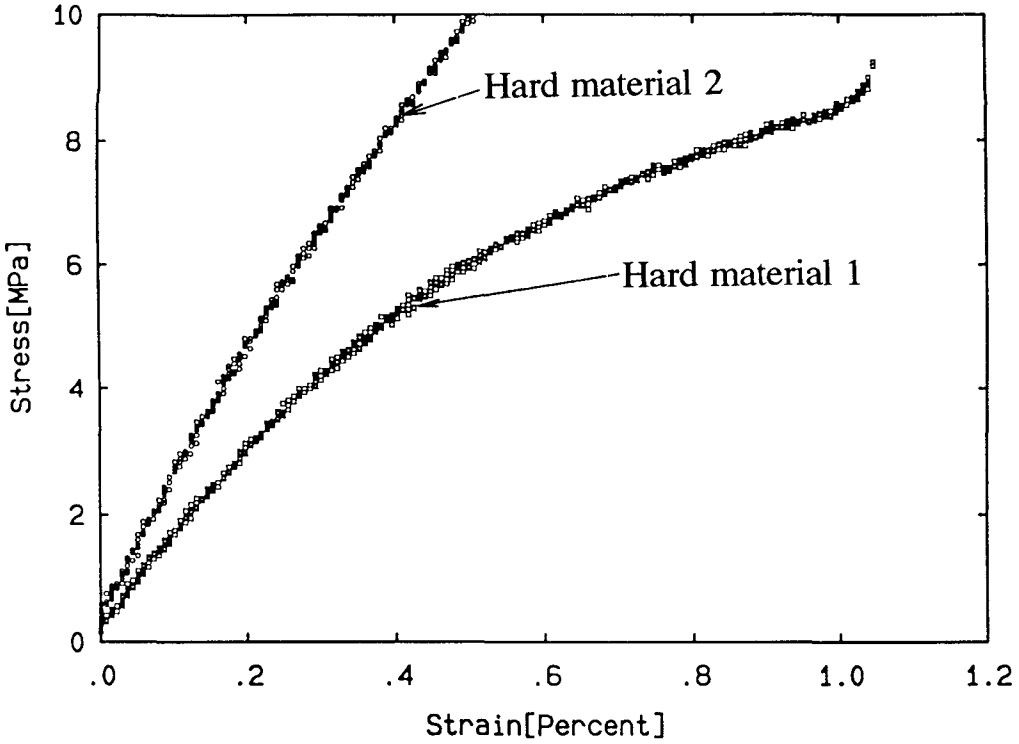

Figure 7.1 Stress-strain relation (Case 8).

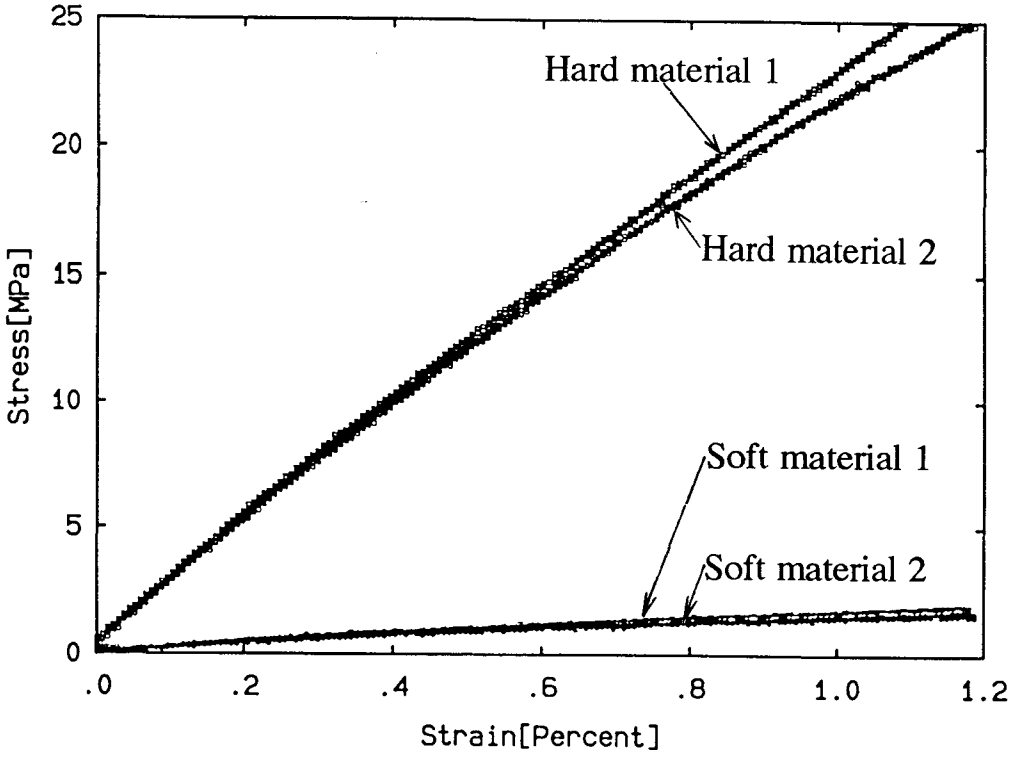

Figure 7.2 Stress-strain relation (Case 9).

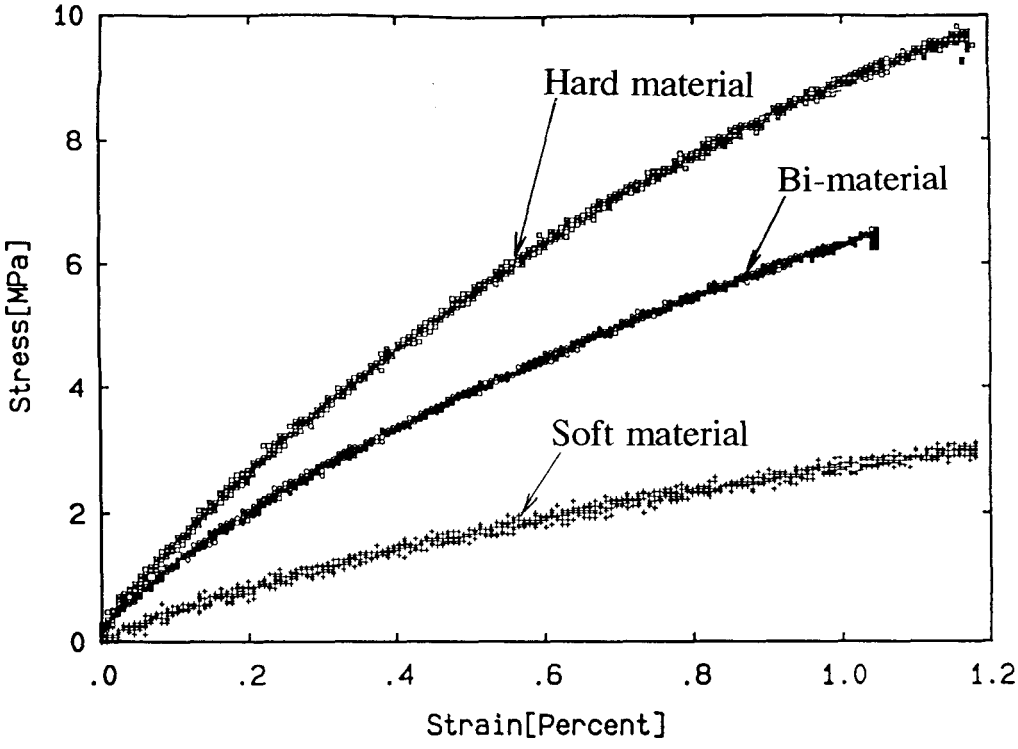

Figure 7.3 Stress-strain relation (Case 1).

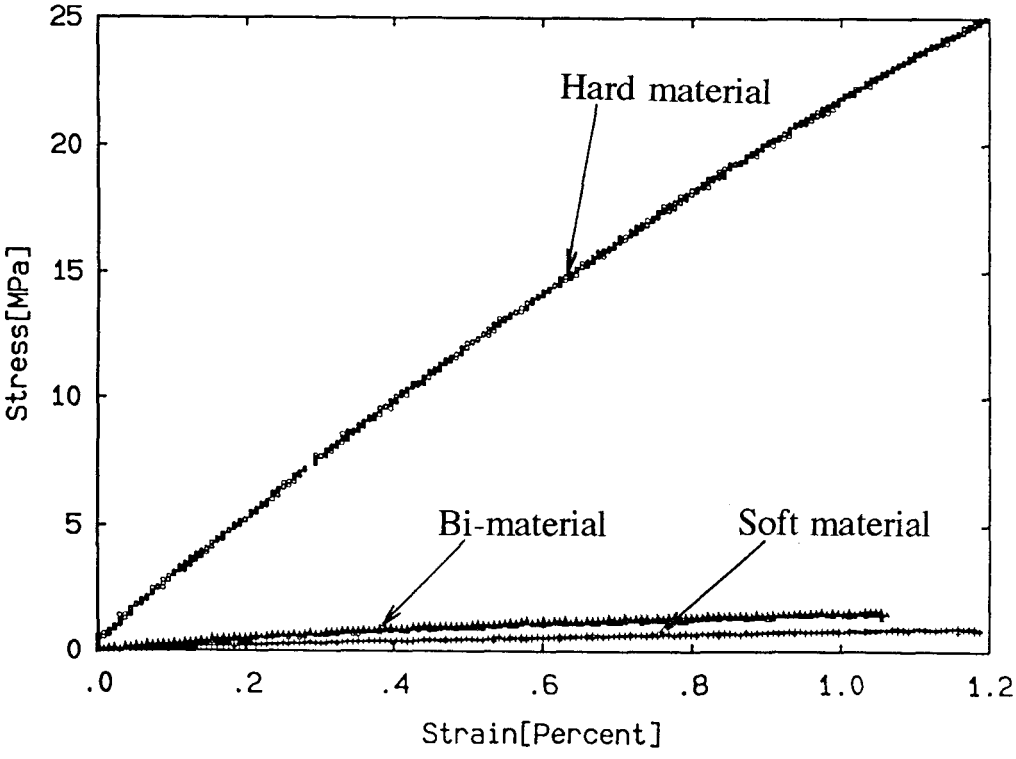

Figure 7.4 Stress-strain relation (Case 8).

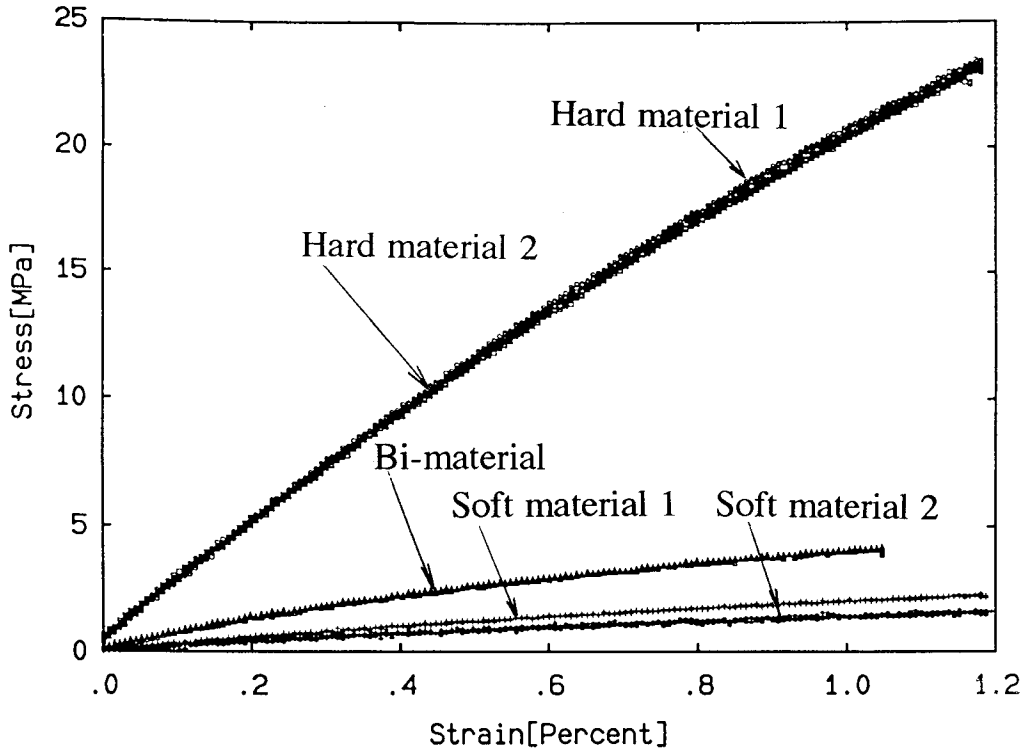

Figure 7.5 Stress-strain relation (Case 10).

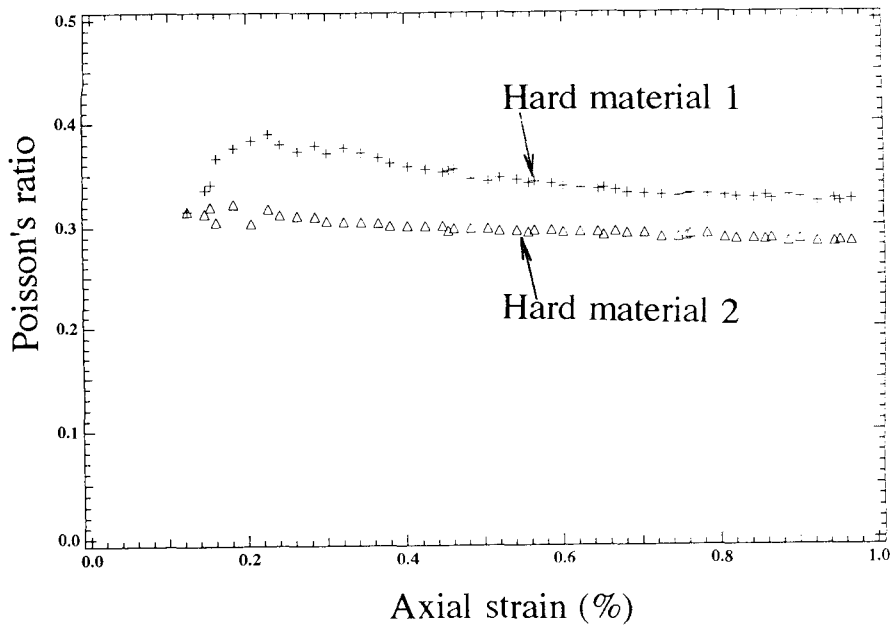

Figure 7.6 (a) Poisson's ratio vs. axial strain obtained using strain gauges (hard material, Case 10).

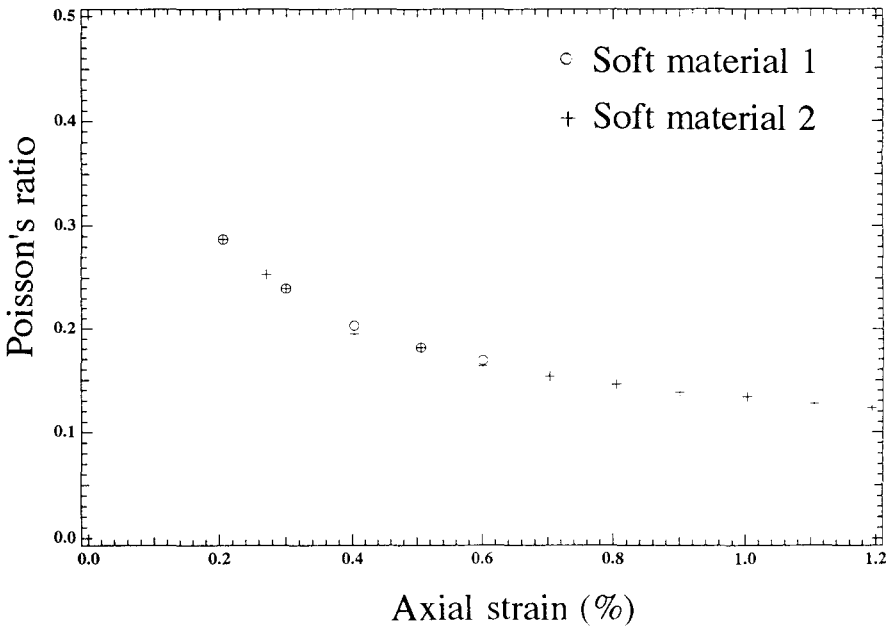

Figure 7.6 (b) Poisson's ratio vs. axial strain obtained using strain gauges (soft material, Case 10)

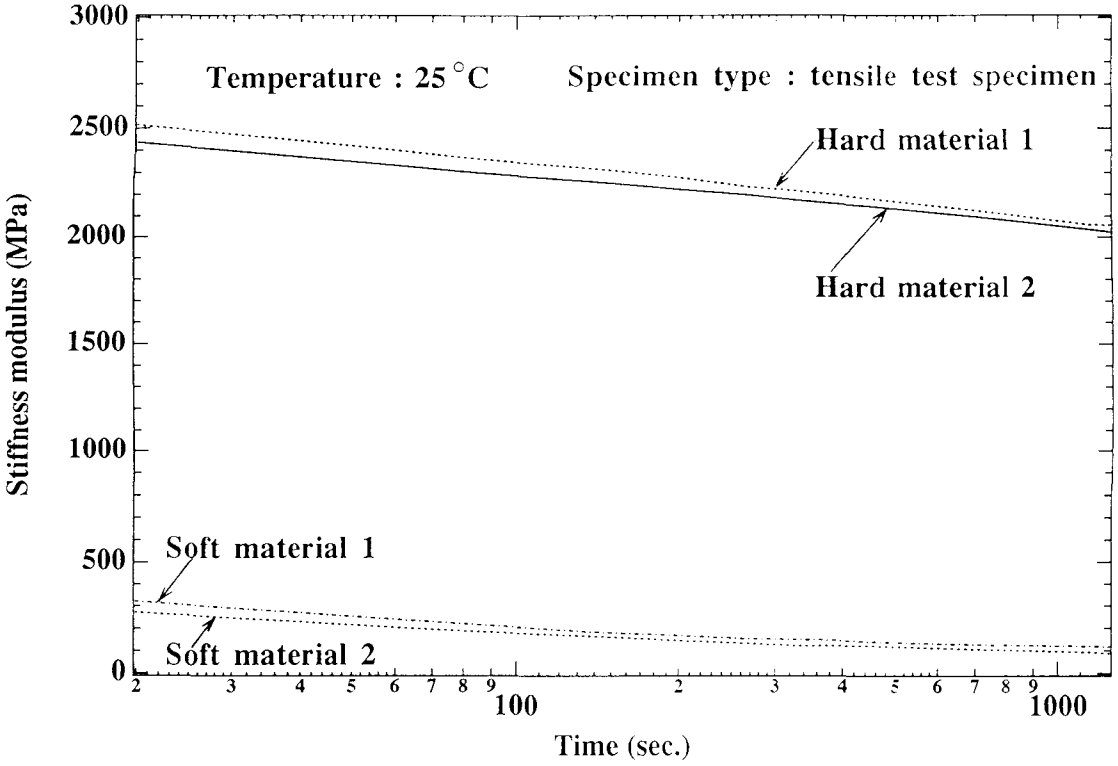

Figure 7.7 Uniaxial tensile stress relaxation (Case 10).

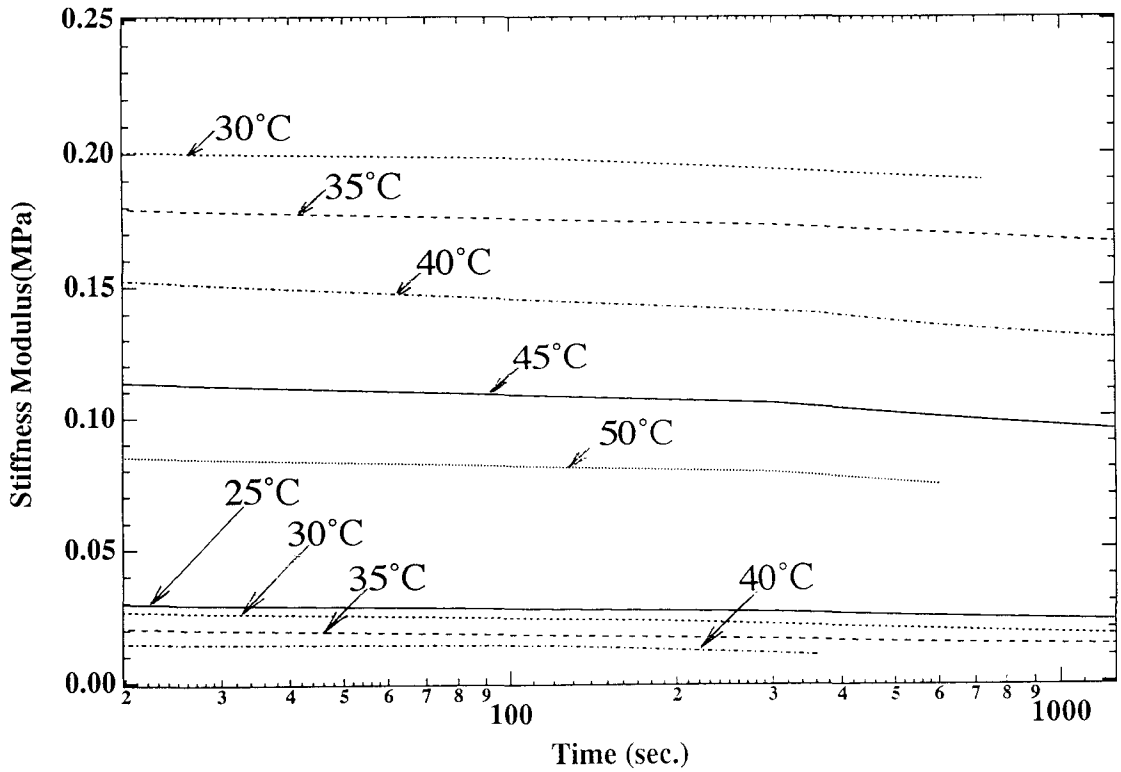

Figure 7.8 Uniaxial stress relaxation (with cracks).

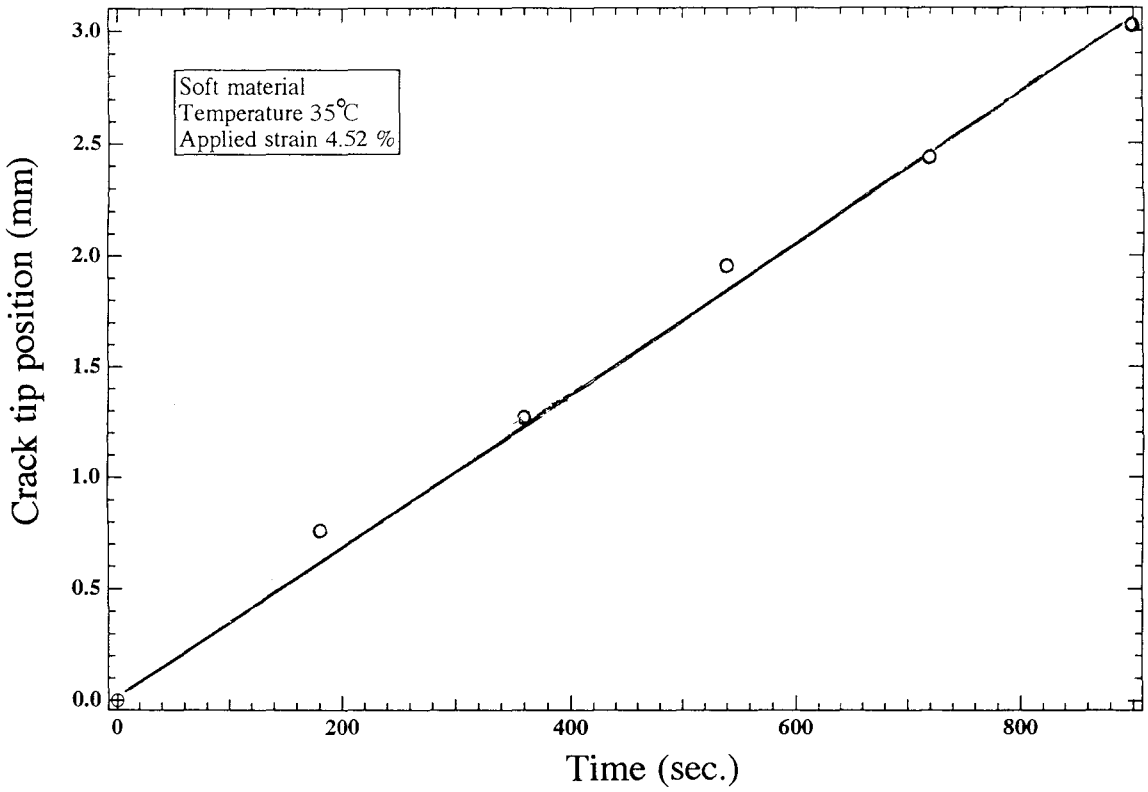

Figure 7.9 Example of data analysis for determining crack speed.

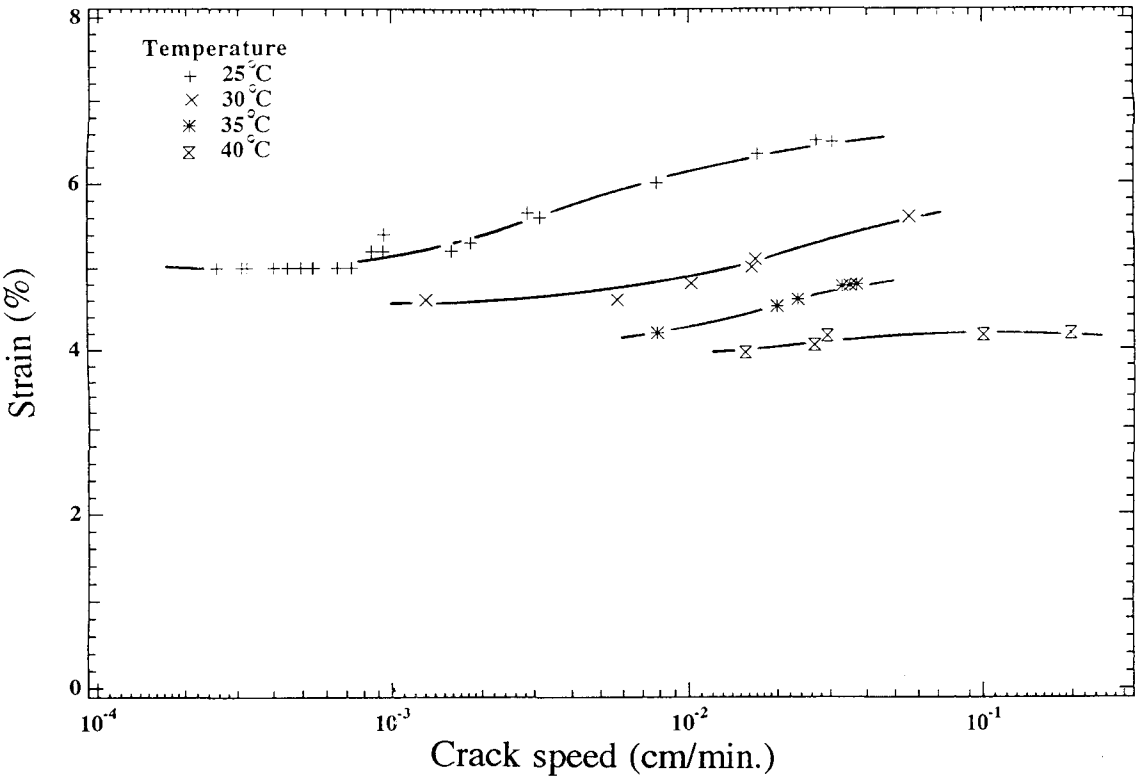

Figure 7.10 (a) Crack velocity as a function of temperature reduced strain (soft material).

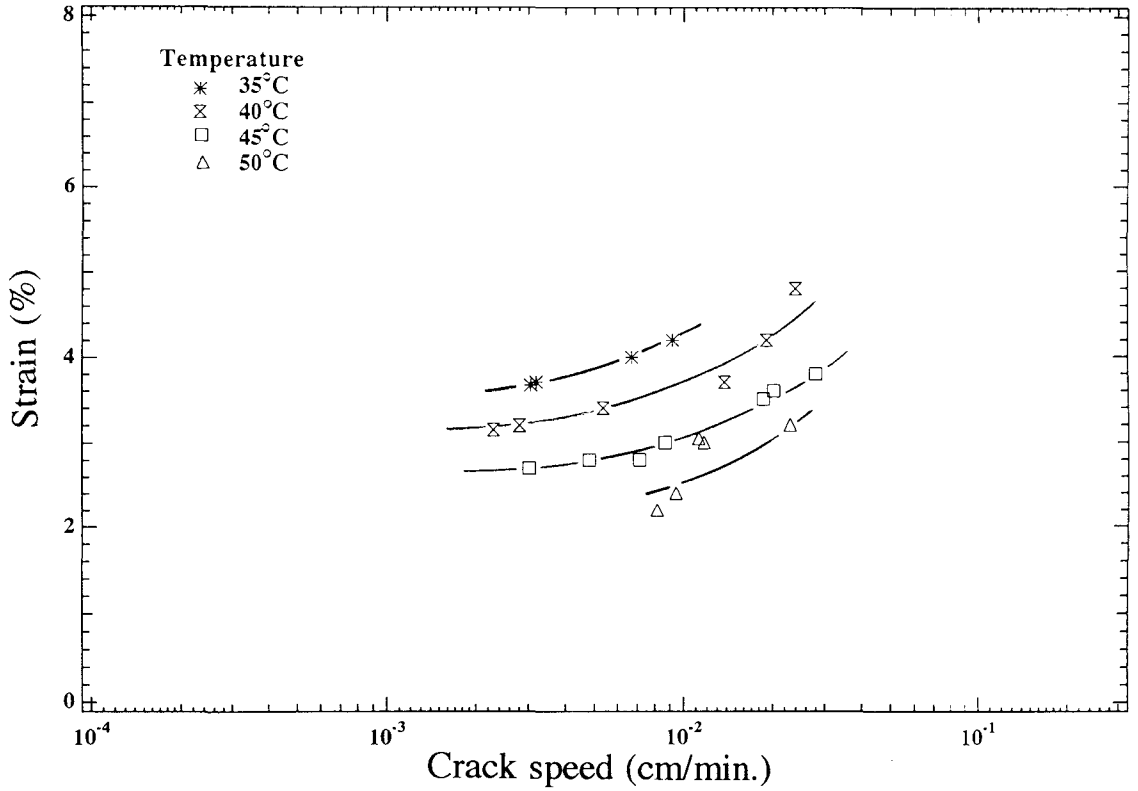

Figure 7.10 (b) Crack velocity as a function of temperature reduced strain (hard material).

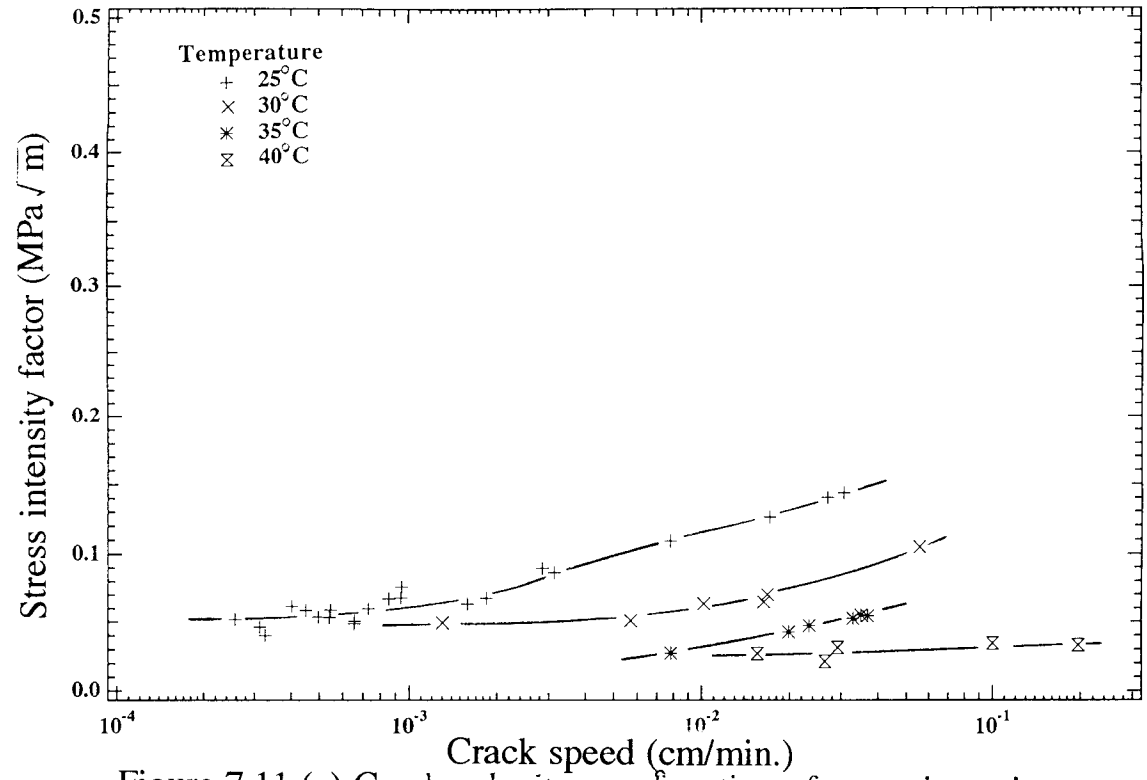

Figure 7.11 (a) Crack velocity as a function of stress intensity factors at several temperatures (soft mat.).

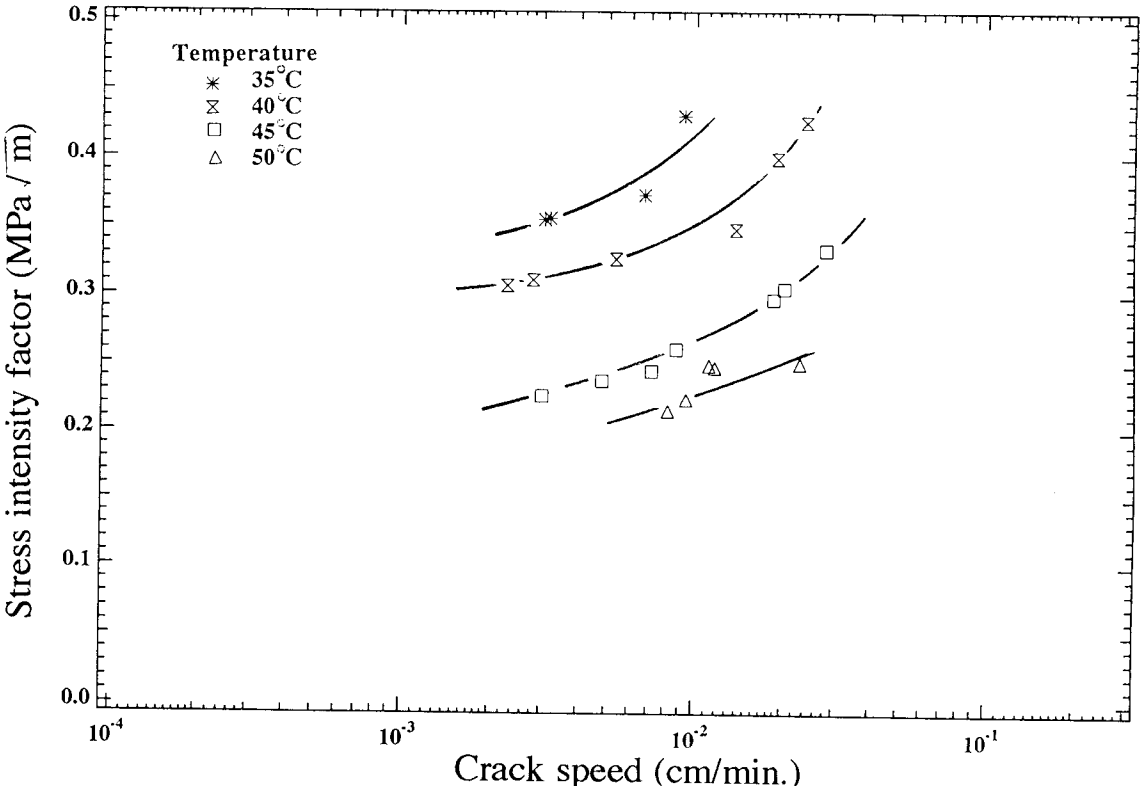

Figure 7.11 (b) Crack velocity as a function of stress intensity factors at several temperatures (hard mat.).

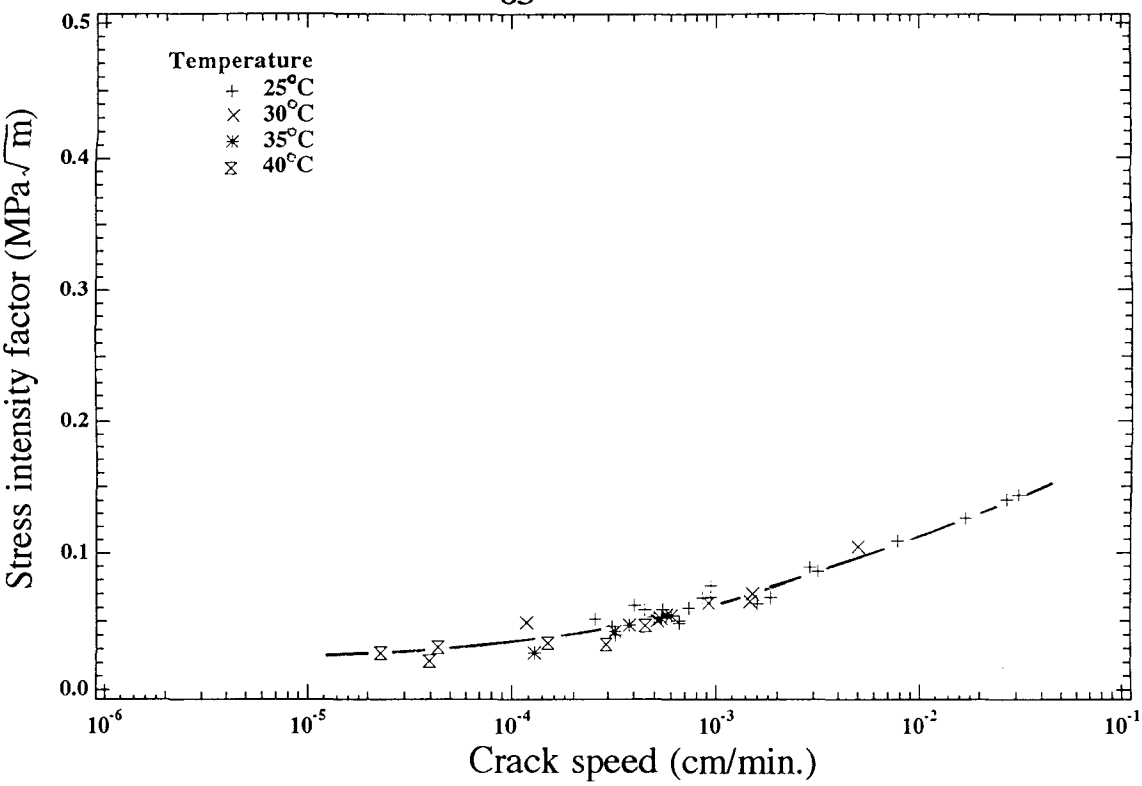

Figure 7.12 (a) Master curve of crack speed derived from Fig. 7.11 (soft material).

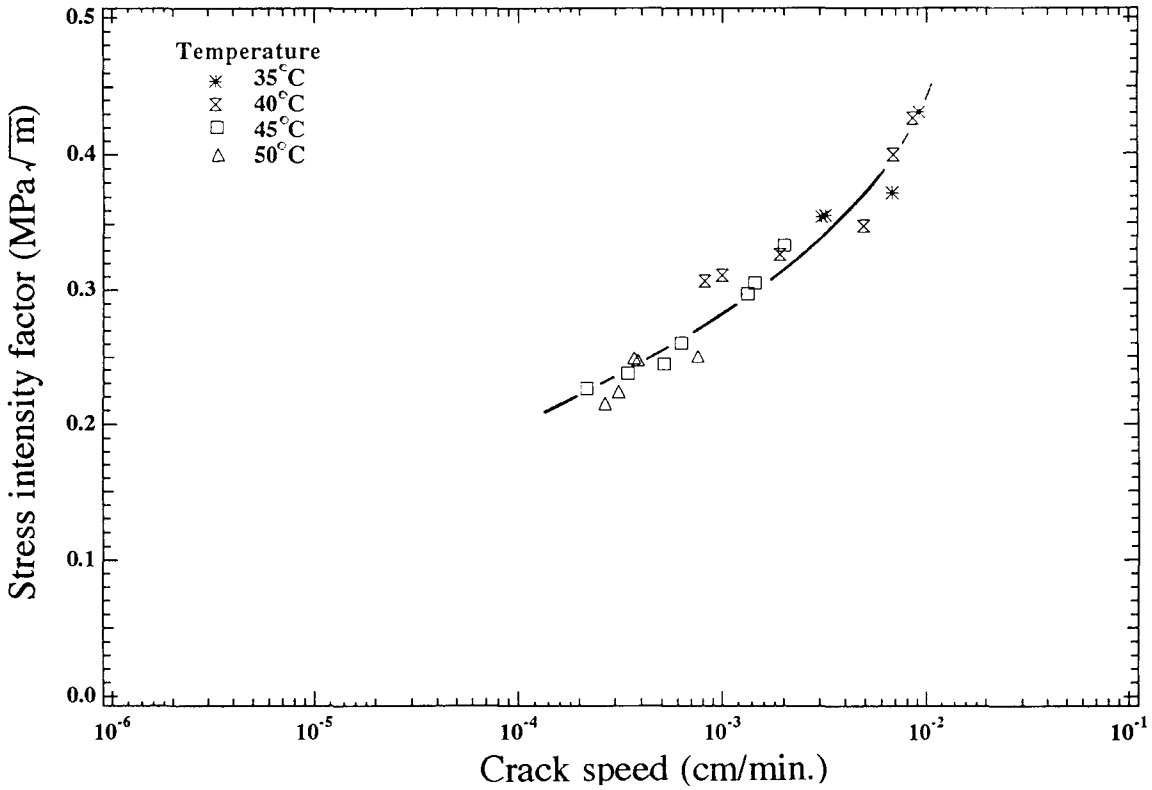

Figure 7.12 (b) Master curve of crack speed derived from Fig. 7.11 (hard material).

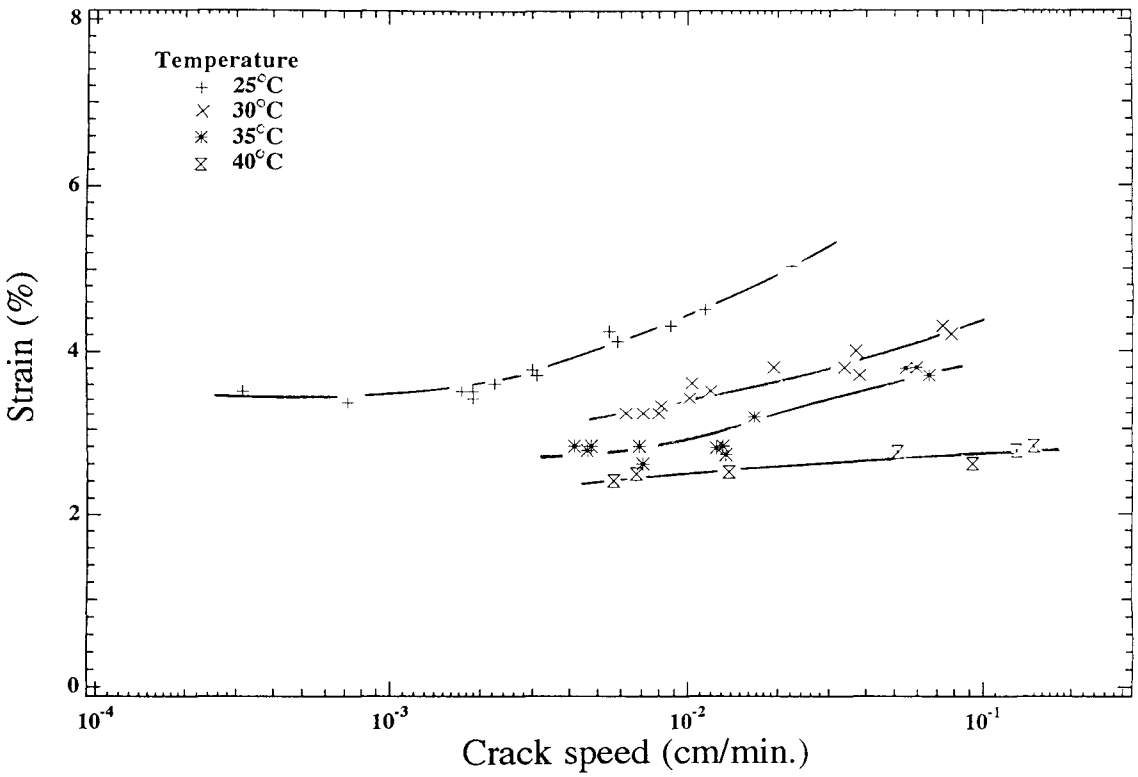

Figure 7.13 Crack velocity as a function of temperature reduced strain.

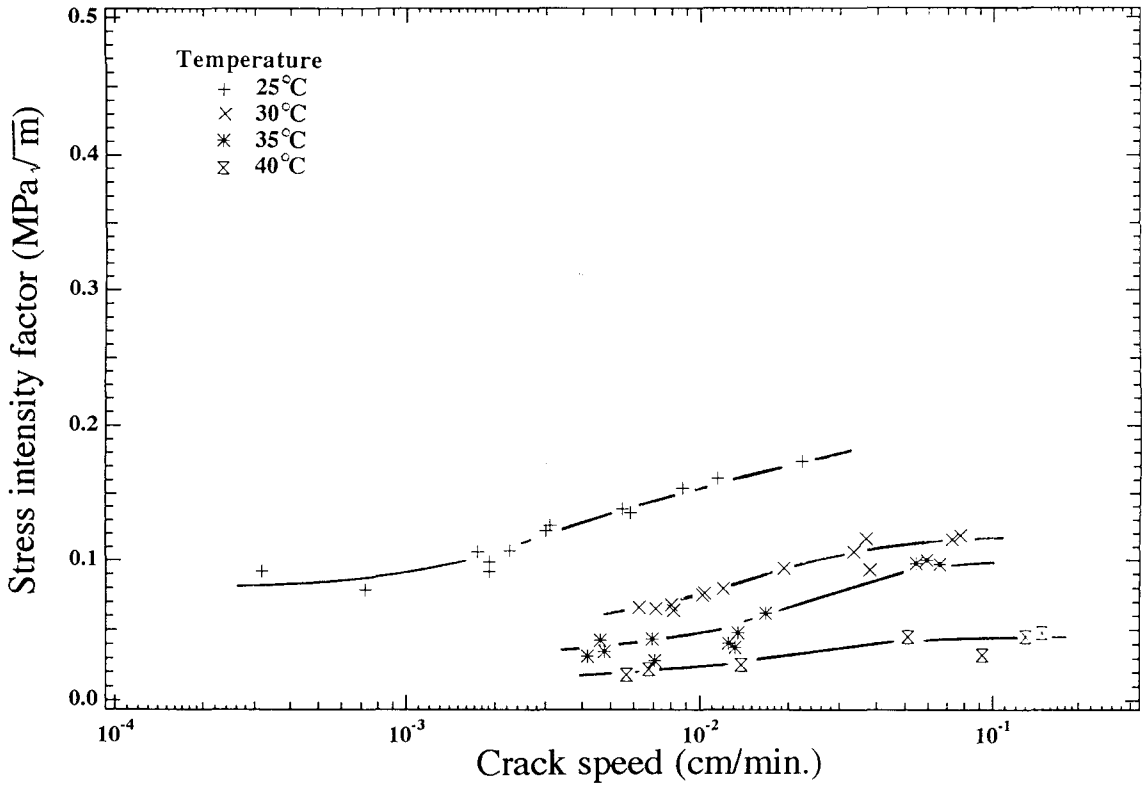

Figure 7.14 Crack velocity as a function of stress intensity factor at several temperatures.

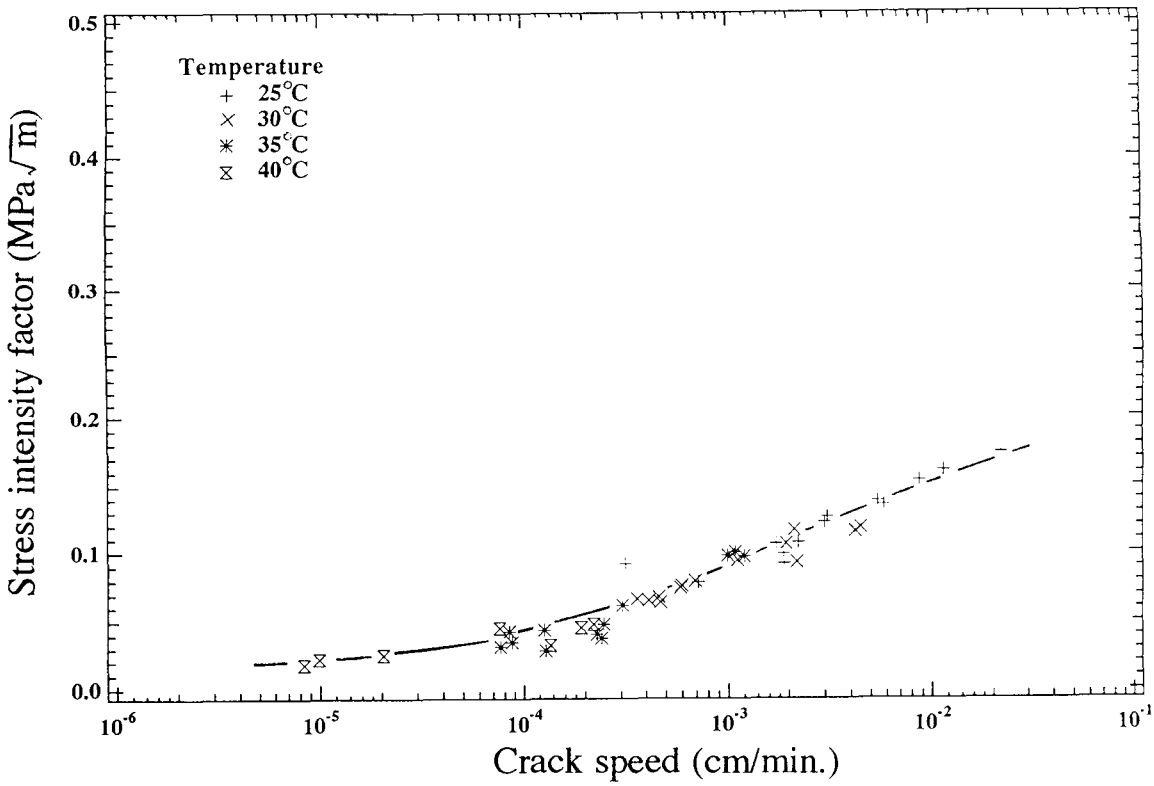

Figure 7.15 Master curve of crack speed derived from Fig. 7.14.

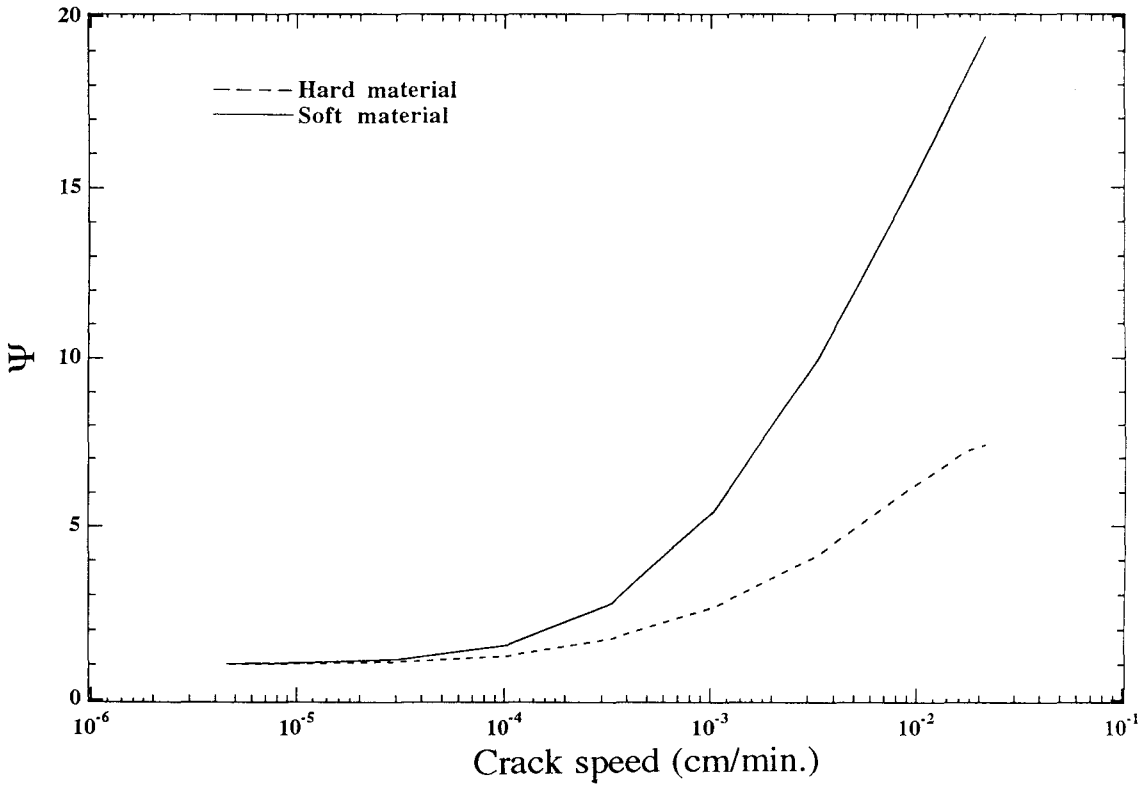

Figure 7.16 The material Ψ functions for the two solids [cf. Eq. (2.8)]

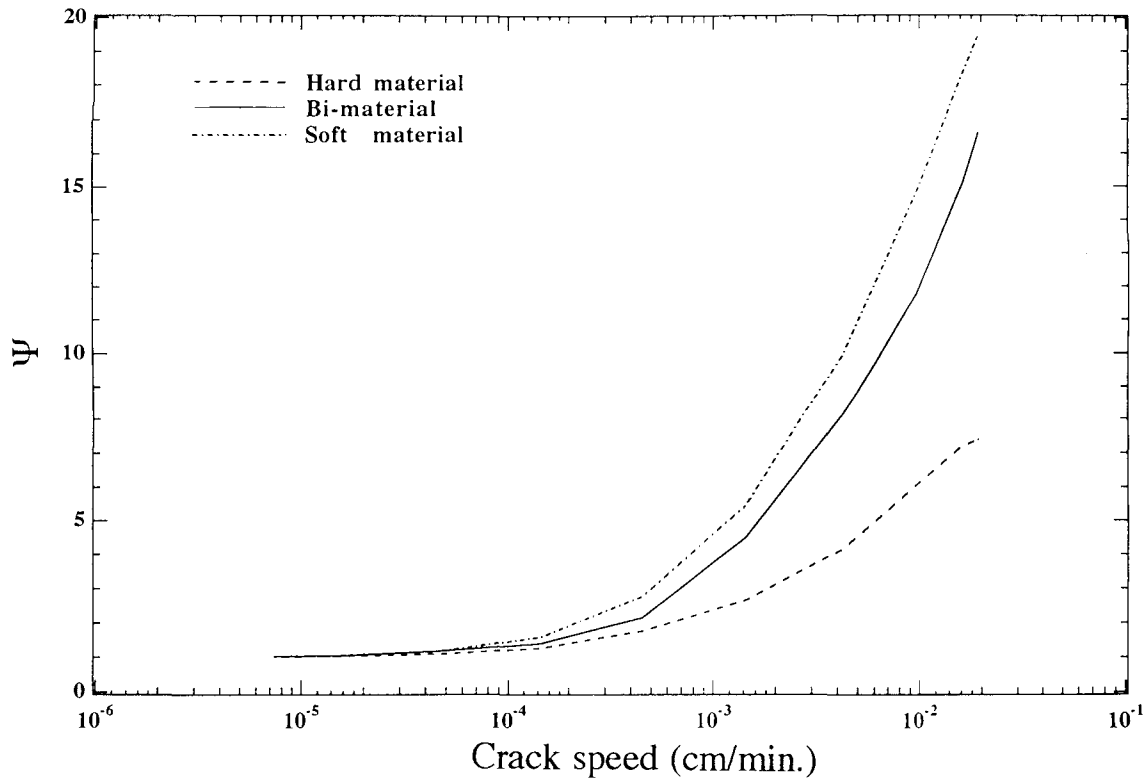

Figure 7.17 The Ψ fuction for bi-material interface fracture.

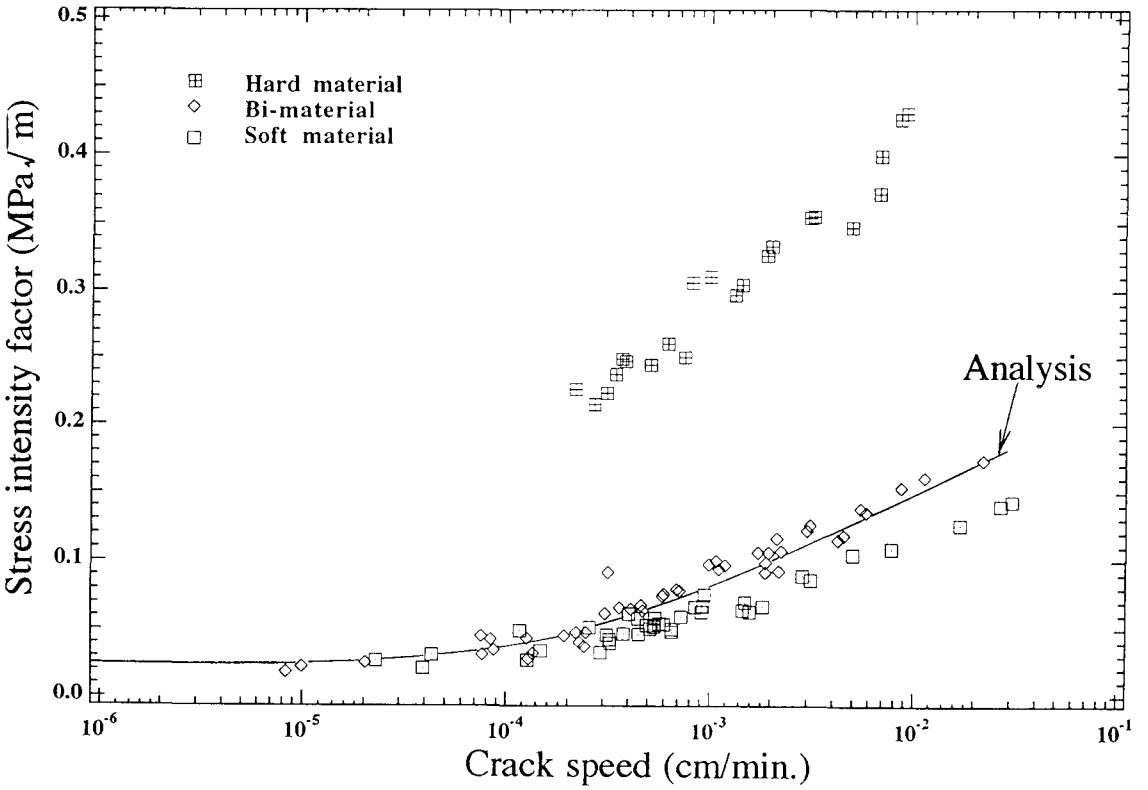

Figure 7.18 Crack propagation speed as a function of the stress intensity factor.

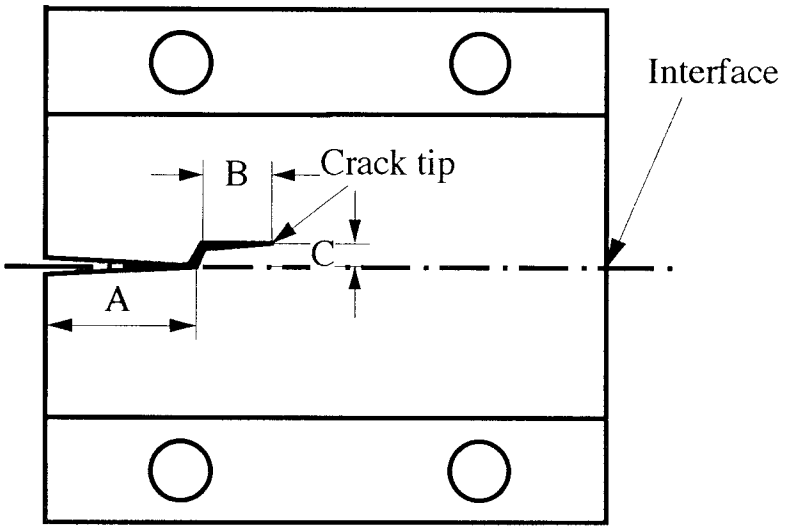

	A	B	C
Soft material	22.96 mm	5.588 mm	2.039 mm
Hard material	21.11 mm	17.22 mm	0.762 mm

Figure 7.19 Geometry of the homogeneous fracture specimen manufactured through a sandwiching process.

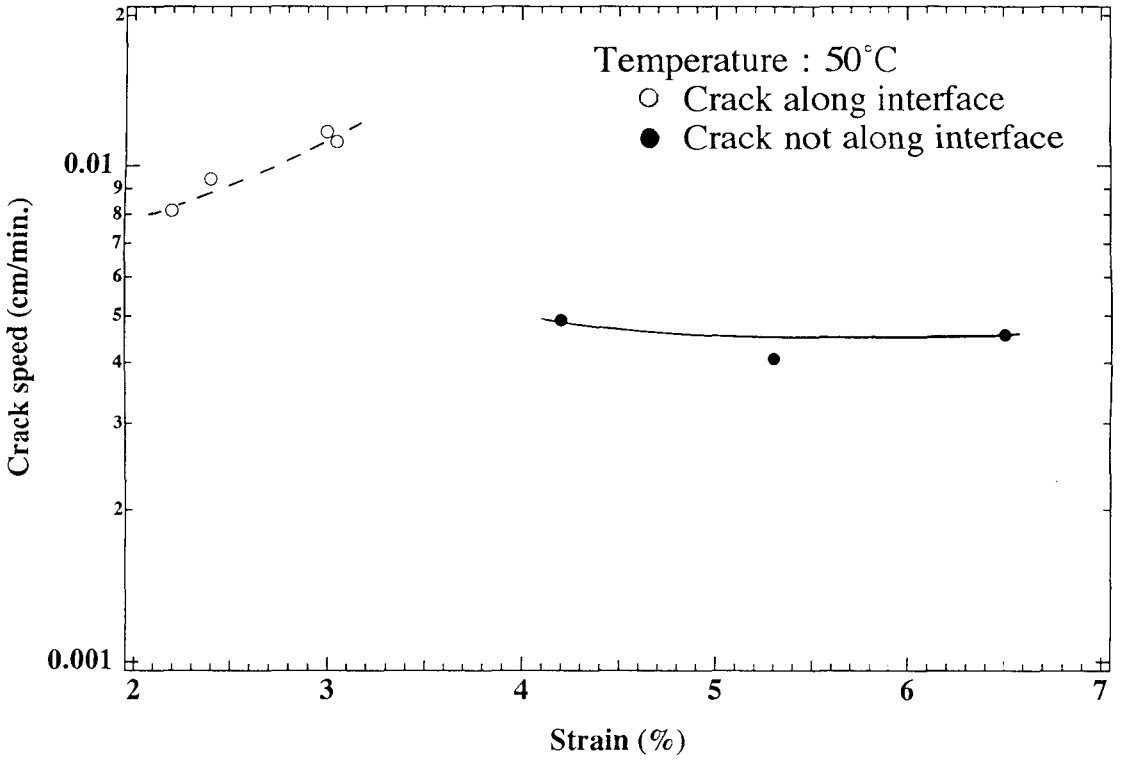

Figure 7.20 (a) Comparison between crack speed and applied strain (hard material).

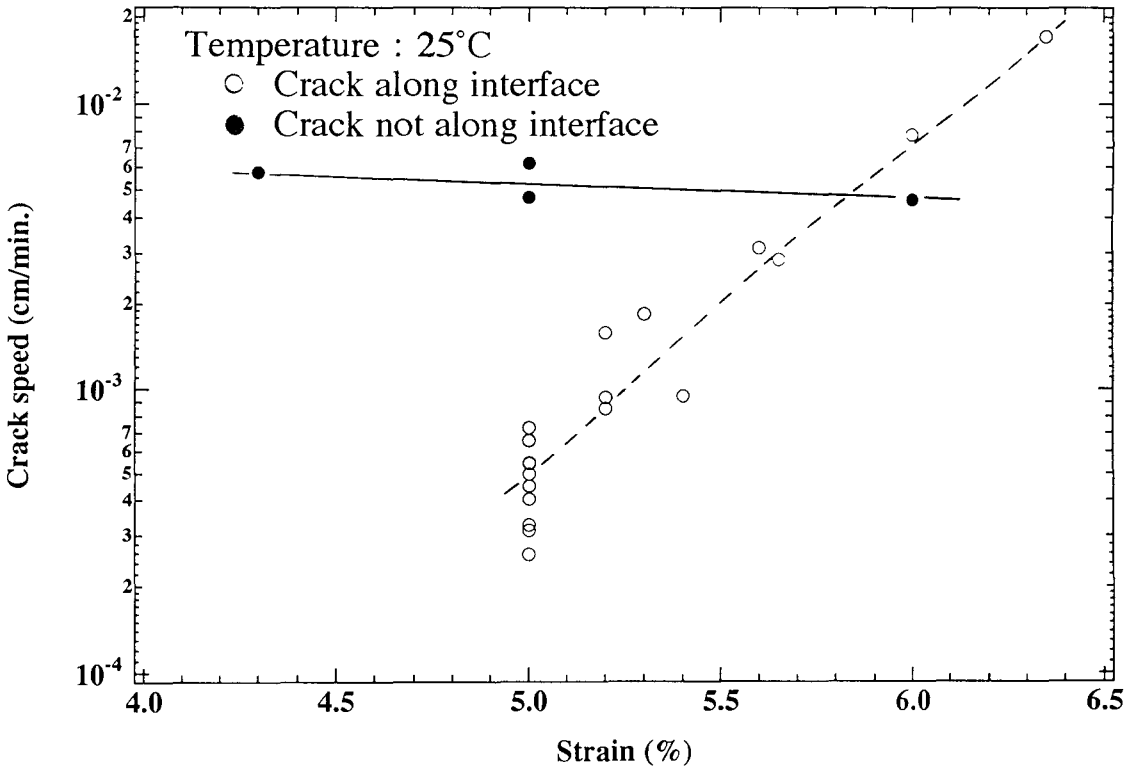

Figure 7.20 (b) Comparison between crack speed and applied strain (soft material).

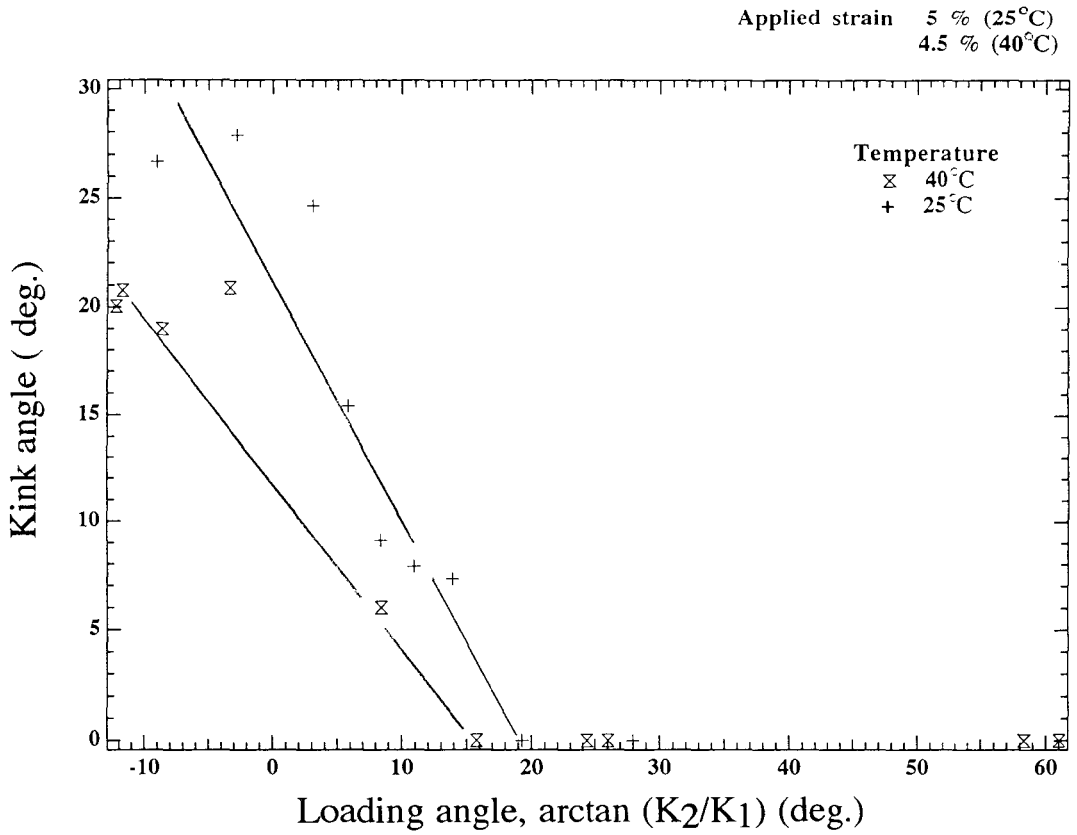

Figure 7.21 Observed kinking behavior of the interface crack.

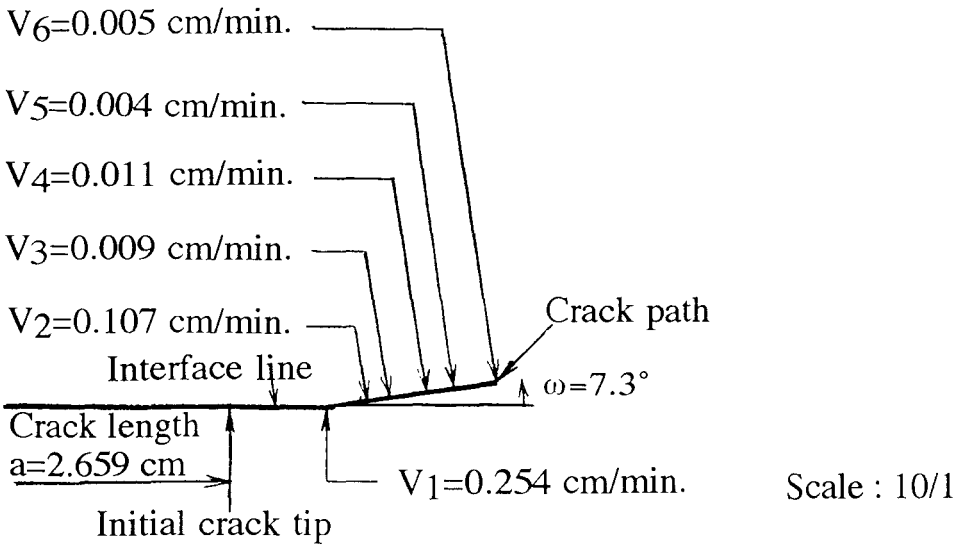

Figure 7.22 (a) Observed crack tip position and crack tip velocity after kinking (25 °C).

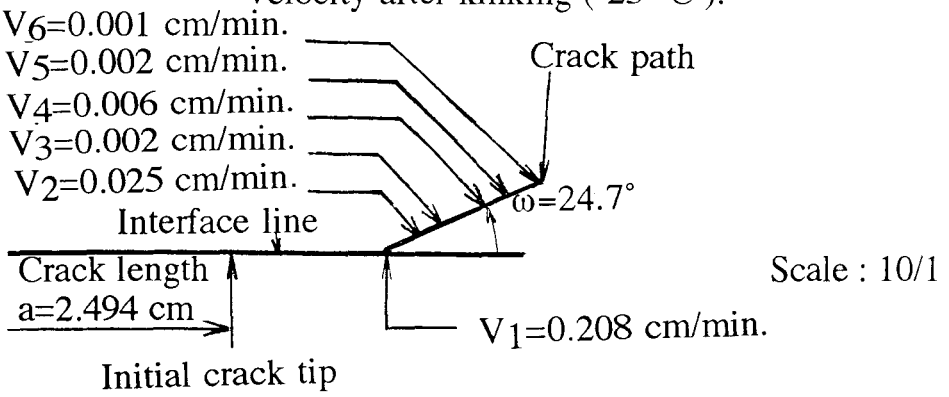

Figure 7.22 (b) Observed crack tip position and crack tip velocity after kinking (25 °C).

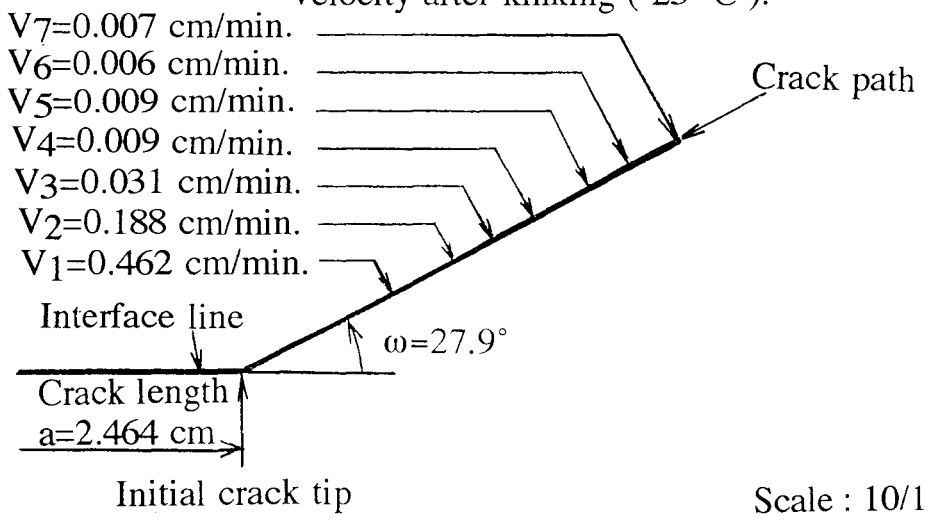

Figure 7.22 (c) Observed crack tip position and crack tip velocity after kinking (25 °C).

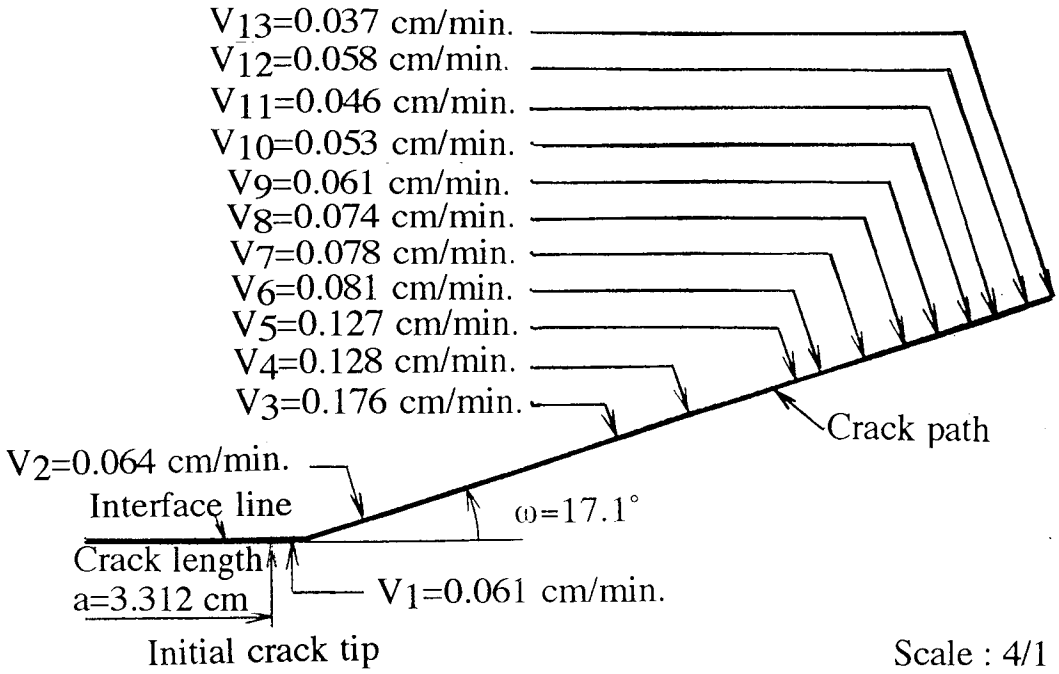

Figure 7.23 (a) Observed crack tip position and crack tip velocity after kinking (40 °C).

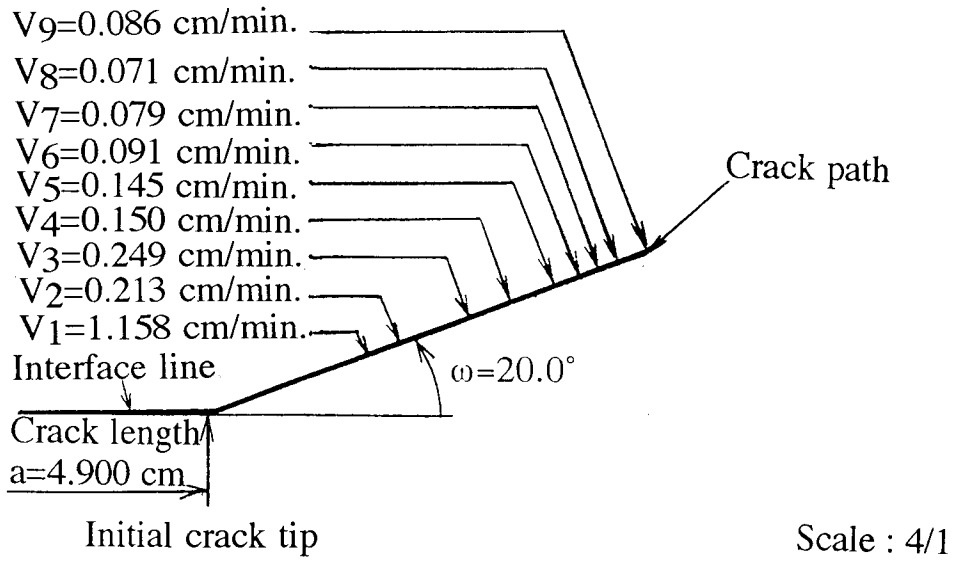

Figure 7.23 (b) Observed crack tip position and crack tip velocity after kinking (40 °C).

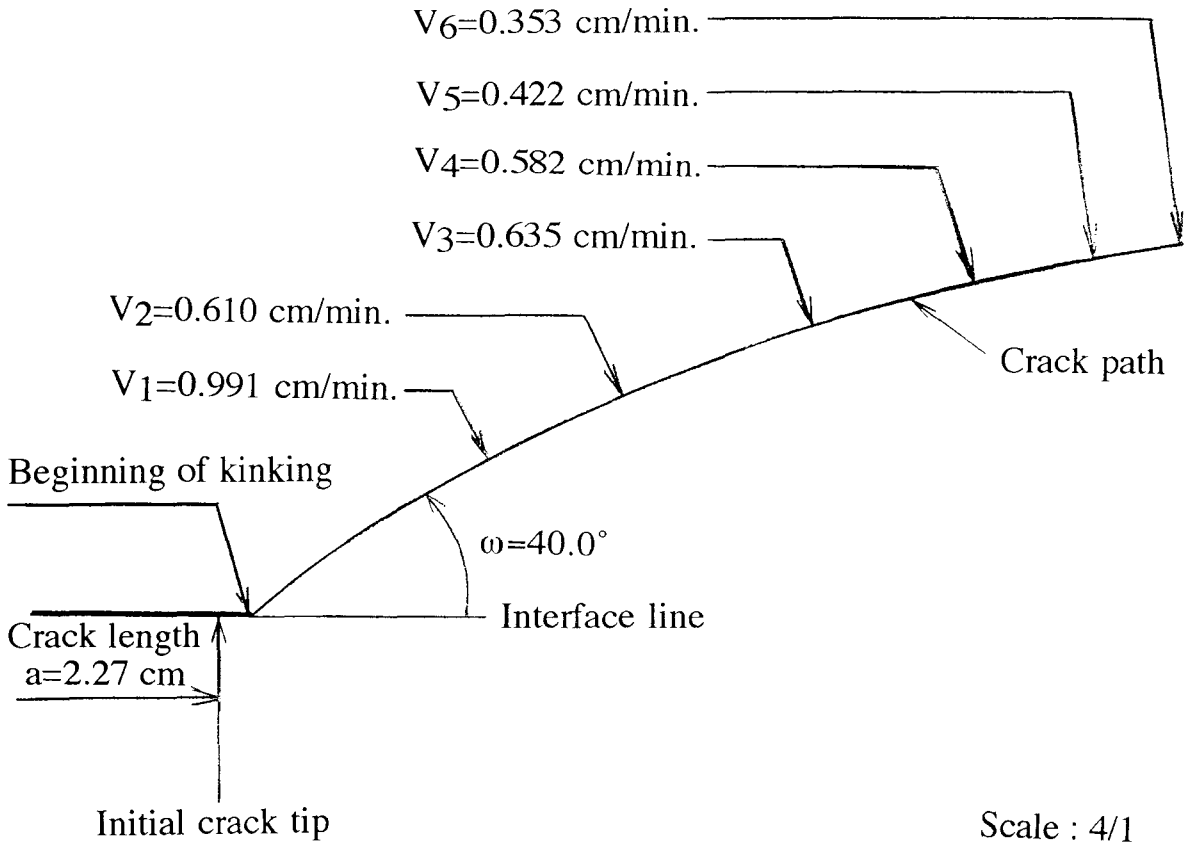

Figure 7.23 (c) Observed crack tip position and crack tip velocity after kinking (40 °C).

8. Conclusions

The growth of a crack located at an interface between two epoxies was investigated experimentally. To study the interfacial crack growth, first, the homogeneous and then bi-material specimens were manufactured with castable liquid epoxy resins. To meet the requirements established in the beginning stage of this research, the manufacturing processes of the bi-material specimen were optimized. One of the difficulties to overcome throughout the manufacturing process was to produce a flat interface. To optimize the various manufacturing processes, the constant deformation rate (stiffness modulus) using the tensile test specimens of the two homogeneous materials and the bi-material were measured and examined. It has been demonstrated that the manufacturing process, which follows previously established procedures for the bi-material solid composed of Solithane, was also applicable to epoxy. The fracture toughness of the interfacial crack was investigated with strip biaxial specimens, for comparison with those of the homogeneous materials. In this evaluation, parameters of the stress intensity factor and crack tip speed were used. The data were plotted as "master curves" for either of the two homogeneous materials and the bi-material. The "master curve" of the bi-material was compared with the expected values of viscoelastic interface failure model proposed by Knauss (1971). It was demonstrated that the above model was applicable to the interfacial crack problem in epoxy solids.

Following the evaluation of the specimen interface toughness, the propensity of the interface crack to kink out of the interface upon loading was investigated. The crack could be made to advance into the soft material or along the interface itself, depending on the character of the applied

loading conditions. Although the number of data points was small, the fracture data gathered from tests performed at 25°C and at 40°C indicated that rate effects significantly influenced the kinking behavior of these joints. However, in these tests kinking into the hard material was not observed.

References

Bowen, J.M., and Mazor, E., 1989, "Crack Propagation At and Near Interfaces of Viscoelastic Solids," *GALCIT Ae 200a Report*, Caltech.

Bowen, J.M., 1990, "Preparation of a Bi-material Fracture Specimen Composed of Solithane 113," *GALCIT SM Report 90-25*, Caltech.

Bowen, J.M., 1992 "An Experimental Investigation of Fracture at a Bimaterial Interface," *Engineering Thesis*, Caltech.

Bowen, J.M., and Knauss, W.G., 1993, "An Experimental Study of Interfacial Crack Kinking," *Experimental Mechanics*, March 1993, pp.37-43.

Dow Chemical Company, 1992, "Improved Elongation, Flexibility, and Impact in Cured Resins," *Products catalog* .

Dundurs, J., 1969, "Edge-bonded Dissimilar Orthogonal Elastic Wedges Under Normal and Shear Loadings," *ASME Journal of Applied Mechanics*, Vol.36, pp. 650-652.

Geubelle, P.H. and Knauss, W.G., 1991, "Crack Propagation At and Near Bimaterial Interfaces : Linear Analysis," *GALCIT SM Report 91-17*, Caltech.

Geubelle, P.H., 1993, "Nonlinear Effects in Interfacial Fracture," *Ph. D Thesis*, Caltech.

Hutchinson, J.W., Mear, M.E., and Rice, J.R., 1987, "Crack Paralleling an Interface Between Dissimilar Materials," *ASME Journal of Applied Mechanics*, Vol.54, pp.828-832.

Knauss, W.G., and Dietmann, H., 1970, "Crack Propagation Under Variable Load Histories in Linearly Viscoelastic Solids," *International Journal of Engineering Science*, Vol.8, pp.643-656.

Knauss, W.G., and Mueller, H.K., 1971, "Crack Propagation in a Linearly Viscoelastic Strip," *Journal of Applied Mechanics*, Vol.38, Series E, p.483.

Knauss, W.G., 1974, " On the Steady Propagation of a Crack in a Viscoelastic Sheet : Experiments and Analysis," *GALCIT SM 73-2*, Caltech.

Knauss, W.G., 1976, "Fracture of Solids Possessing Deformation Rate Sensitive Material Properties," *The Mechanics of Fracture*, F. Erogen, ed., ASME, NY, AMD Vol.19.

Knauss,W.G., 1988, "An Investigation of Viscoelastic Fracture Near and At Interfaces," *GALCIT SM 88-13*, AFAL-TR-88-083, Caltech.

Matos,P.P.L., McMeeking, R,M., Charalambides, P.G., and Drory, M.D., 1989, "Method for Caluculating Stress Intensities in Bimaterial Fracture," International Journal of Fracture, Vol.40, pp.235-254.

Mazor, E. and Bowen, J.M., 1990, "Material Selection : An Investigation of the Mechanical Properties and the Aging Behavior of Solithane 113," *GALCIT Ae200b Report*, Caltech.

Mukai, D.J., Ballarini, R., and Miller, G.R., 1990, "Analysis of Branched Interface Cracks," *ASME Journal of Applied Mechanics*, Vol.57, pp.887-893.

Rice, J.R., 1899, "Elastic Fracture Mechanics Concepts for Interfacial Cracks," *ASME Journal of Applied Mechanics*, Vol.55,pp.98-103.

Sugawara, S., 1993, "Preparation of a Bi-material Fracture Specimen Composed of Epoxy," *GALCIT Ae200b Report*, Caltech.

Sugawara, S., 1993, "Tensile Test results of a Bi-material Fracture Specimen Composed Epoxy," *GALCIT Ae200c Report*, Caltech.

Sun, C.T., and Jih, C. J.,1987, "On Strain Energy Release Rates for Interfacial Cracks in Bi-material Media," *Engineering Fracture Mechanics*, Vol.28 No.1, pp.13-20.